A Simple Computational Proxy for Screening Magnetocaloric Compounds

Joshua D. Bocarsly,[†,‡] Emily E. Levin,[†,‡] Christina A. C. Garcia,[¶] Kai Schwennicke,[§] Stephen D. Wilson,[‡,†] and Ram Seshadri[*,‡,†,‖]

†*Materials Department, University of California, Santa Barbara, California 93106, United States*

‡*Materials Research Laboratory, University of California, Santa Barbara, California 93106, United States*

¶*Physics Program, College of Creative Studies, University of California, Santa Barbara, California 93106, United States*

§*Chemistry Program, College of Creative Studies, University of California, Santa Barbara, California 93106, United States*

‖*Department of Chemistry and Biochemistry, Santa Barbara, California 93106, United States*

E-mail: seshadri@mrl.ucsb.edu

Abstract

Alternating cycles of isothermal magnetization and adiabatic demagnetization applied to a magnetocaloric material can drive refrigeration in very much the same manner as cycles of gas compression and expansion. The material property of interest in finding candidate magnetocaloric materials is their gravimetric entropy change upon application of a magnetic field under isothermal conditions. There is, however, no general method of screening materials for such an entropy change without actually carrying out the relevant, time- and effort-intensive magnetic measurements. Here we propose a simple computational proxy based on carrying out non-magnetic and magnetic density functional theory calculations on magnetic materials. This proxy, which we refer to as the magnetic deformation Σ_M, is a measure of how much the unit cell deforms when comparing the relaxed structures with and without the inclusion of spin polarization. Σ_M appears to correlate very well with experimentally measured magnetic entropy change values. The proxy has been tested against 33 known ferromagnetic materials, including nine materials newly measured for this study. It has then been used to screen 134 ferromagnetic materials for which the magnetic entropy has not yet been reported, identifying 30 compounds as being promising for further study. As a demonstration of the effectiveness of our approach, we have prepared one of these compounds and measured its isothermal entropy change. MnCoP, with $T_C = 575\,\mathrm{K}$, shows a maximum $\Delta S_M = -6.0\,\mathrm{J\,kg^{-1}\,K^{-1}}$ for an applied field of $H = 5\,\mathrm{T}$.

Introduction

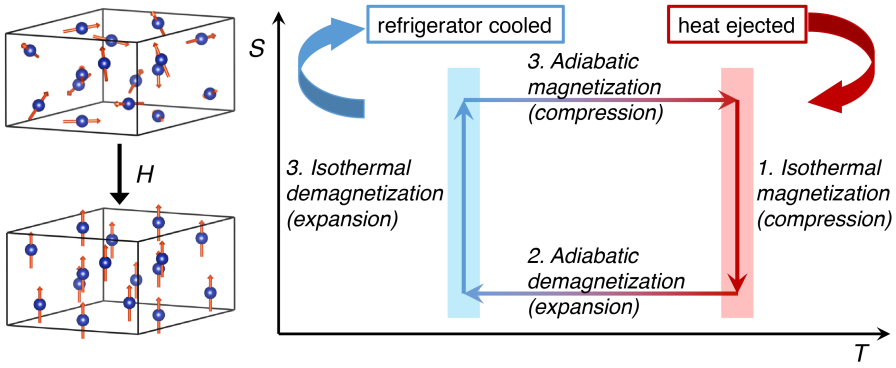

Figure 1: Illustration of the Carnot cycle for magnetic refrigeration, which is analogous to the conventional vapor-compression cycle.

Magnetic refrigeration, based on the magnetocaloric effect (MCE),[1] has been proposed as an energy efficient and environmentally friendly alternative to vapor compression refrigeration.[2] In a typical ferromagnet near its Curie temperature, application of a magnetic field, H, causes randomly oriented spins to align, leading to a decrease in magnetic entropy of the material, as depicted in Figure 1. If this magnetization is performed adiabatically, the decrease in magnetic entropy is compensated by a rise in temperature, and *vice-versa* for demagnetization. If the magnetization is performed isothermally, the material will decrease its total entropy and reject heat. By alternating adiabatic and isothermal magnetizations and demagnetizations, one can use the magnetocaloric effect to drive a thermodynamic cycle in direct analogy to the conventional vapor-compression cycle. With the use of a regenerator, this process can cool with a large coefficient of performance near room temperature.[3,4] Developments in magnetocaloric materials and in magnetic refrigerator engineering over the past several years have lead to the first prototype systems, and several companies are promising a new generation of energy-efficient refrigerators and air conditioners in the near future.[5,6]

To evaluate a magnetocaloric material, the isothermal entropy change $\Delta S_M(T, H)$ and adiabatic temperature change $\Delta T_{\mathrm{ad}}(T, H)$ are typically the first parameters investigated.

These two parameters represent the height and width, respectively, of the Carnot cycle diagram shown in Figure 1. For magnetic refrigeration near room temperature, several suitable materials are being studied in detail, including $(Mn,Fe)_2(P,Si)$,[7,8] $La(Fe,Si)_{13}$ and its hydrides,[9] and Heusler compounds.[10,11] These systems are comprised of Earth-abundant, inexpensive elements and combine large ΔS_M and ΔT_{ad}, with low hysteresis, high mechanical and chemical stability, and good thermal properties. Despite great progress within these systems, discovery of new magnetocalorics with desirable properties is still important. As the first generation of magnetocalorics moves towards commercial viability, more and more diverse applications of the magnetocaloric effect are being proposed, including gas liquefaction,[12] small-scale solid state cooling,[13] and thermomagnetic generators.[14] These applications will each demand materials with different properties, including a range of active temperatures, cycling properties, thermal properties, and magnetic field responses.

Various competing interactions contribute to the magnetocaloric effect, creating challenges in the discovery of new magnetocaloric materials. The first materials investigated for magnetic cooling near room temperature were ferromagnets with standard second-order paramagnetic to ferromagnetic phase transitions. The most common metric used to search for new materials is the saturation magnetization, M_S: materials with a high density of polarized spins are expected to show larger changes in entropy. For this reason, Gd, which has a saturation magnetization in excess of 250 emu/g and a Curie temperature near room temperature,[15] is the prototypical second order material. Indeed, Gd shows a sizeable magnetic entropy change of $6.1\,\mathrm{J\,kg^{-1}\,K^{-1}}$ and adiabatic temperature change of 6.4 K for an applied field $H = 2\,\mathrm{T}$.[16] Phenomenological models can be used to describe the entropy change in these materials, but these models are descriptive rather than predictive.[17,18]

The discovery of a "giant" magnetic entropy change in $Gd_5(Si,Ge)_4$ in 1997 created new opportunities in the search for magnetocalorics. In $Gd_5(Si,Ge)_4$, a first-order coupled

magnetic and structural transition leads to a greatly enhanced ΔS_M.[19–21] After the discovery of this phenomena, several other systems with known first-order magnetostructural transitions were investigated, yielding some of the most promising magnetocaloric materials, including Fe_2P-based and $La(Fe,Si)_{13}$-based materials. In these systems, coupling of the spins and the lattice leads to a system with switchable magnetostructural state, so that a moderate magnetic field can induce a large change in the magnetic entropy of the system.[18,20,22]

Inspired by these ideas, we propose here the use of computational screening to aid in discovery of new magnetocalorics. Recently, several high-throughput projects have used density functional theory (DFT) to calculate the total energies and electronic structures of hundreds of thousands of known and hypothetical materials.[23–25] Many physical properties can be easily and reliably calculated with DFT. For more complicated properties such as the magnetocaloric effect, it is advantageous to design a computational "proxy" that correlates well with experimental results. The strategy of using proxies has been employed in the search for thermoelectrics,[26] phosphors,[27] and battery materials.[28–30] The screening parameter is, in each case, designed based on physical understanding and is verified against relevant experimental observations before being used to identify materials that merit further experimental or computational study.

Here, we introduce the magnetic deformation Σ_M, a simple DFT-based proxy for screening of new magnetocalorics. The experimental ΔS_M is shown to correlate well with Σ_M across the full range of investigated transition metal-based magnetocalorics. We use Σ_M to screen 134 ferromagnetic materials that have not yet been characterized for magnetocaloric effect, identifying 30 candidates for further experimental study. As a preliminary validation of this strategy, we show magnetocaloric measurements on one of these candidates, MnCoP. MnCoP shows a peak ΔS_M of $-6.0\,\mathrm{J\,kg^{-1}\,K^{-1}}$ for an applied field of $H = 5\,\mathrm{T}$ near its Curie temperature of $T_C = 575\,\mathrm{K}$. This entropy change is much larger than expected for a typical ferromagnet, and MnCoP fits nicely into the trend of ΔS_M *vs.* Σ_M

established in this study. In carrying out this investigation, we have aggregated experimental data and performed calculations on more than 160 magnetic materials, which can potentially aid in data-driven approaches for materials screening.

Methods

Data aggregation

A search of the scientific literature for magnetocaloric materials yielded 24 reported compounds and associated crystal structures, transition temperatures and maximum isothermal magnetic entropy changes, ΔS_M, for applied fields of 2 T and 5 T. We have restricted this dataset to rare earth-free materials with simple unit cells that display ferromagnetic to paramagnetic transitions. In this case, simple unit cells means unit cells that do not contain atomic site disorder, and are therefore straightforward to model with DFT using periodic boundary conditions. In some instances where the reported unit cells contained atomic site disorder in the form of multiple atoms randomly mixed on a single crystallographic site, an ordered approximation of the unit cell was used. For example, (Mn,Fe)$_2$(P,Si) compounds are well-known to contain some mixing of Mn and Fe atoms and P and Si atoms;[31] however, MnFeP$_{2/3}$Si$_{1/3}$ was still included in the dataset because a reasonable approximate unit cell is generated by assuming all of the the Mn is ordered on the $3g$ site, the Fe on the $3f$ site, the P on the $2c$ site, and the Si on the $1b$ site. Compounds containing rare earth atoms (except Y and La) were not included in this study due to difficulties in accurately modeling f-electrons with DFT.

This dataset naturally contains a bias towards materials with large ΔS_M because poorer performing materials are seldom reported. Consequently, we supplemented the data set with new ΔS_M measurements on nine ferromagnetic materials, including several with low ΔS_M values. These values were obtained from magnetic measurements via the Maxwell relation:

$$\left(\frac{\partial S}{\partial H}\right)_T = \left(\frac{\partial M}{\partial T}\right)_H \quad (1)$$

This relation allows for the calculation of isothermal entropy change using:

$$\Delta S_M(H,T) = \int_0^H \left(\frac{\partial M}{\partial T}\right)_{H'} dH' \quad (2)$$

The temperature derivatives required by this equation were calculated from smoothed magnetization *vs.* temperature curves collected at different magnetic fields between 0.1 T and 5 T using a Quantum Design DynaCool PPMS equipped with a Vibrating Sample Magnetometer (VSM) with a high-temperature oven option. The measured materials are shown in the latter half of Table 1. Ni and Fe_2P were purchased, $FeRu_2Sn$ was prepared as reported in a prior report,[32] and all others were prepared for this study. Details of the preparations and full ΔS_M measurements for these materials are provided in the Supporting Information. In addition to these 33 materials with known ΔS_M, we aggregated the crystal structures and Curie temperatures of 134 transition metal-based ferromagnets with known Curie temperatures (Table 2, Supporting Information Table S2) that have not yet been studied for magnetocaloric performance.

One of the materials we prepared and measured, MnCoP, was chosen because it was predicted to show a strong magnetocaloric effect based on the analysis performed in the present study. The details of the preparation may be found in the Supporting Information, along with a synchrotron X-ray diffraction structural characterization of the sample. The diffraction pattern was taken on the High Resolution Powder Diffraction beamline (11-BM) at the Advanced Photon Source, Argonne National Laboratory and was analyzed by Rietveld refinement using the software packages GSAS[33] and EXPGUI.[34] The crystal structure of MnCoP was drawn using the program VESTA.[35]

Density functional theory calculations

For the materials studied, optimized structures were obtained using density functional theory (DFT) with and without spin-polarization, corresponding to a collinear ferromagnetic state and a nonmagnetic state, respectively. These calculations were performed using the *Vienna ab initio simulation package* (VASP)[36] using projector augmented wave (PAW) psuedopotentials[37,38] within the Perdew-Burke-Ernzerhor (PBE) generalized gradient approximation (GGA).[39] Spin-orbit coupling was not included. The Python packages `pymatgen` and `custodian` were used to build a Python framework to automate, manage, and analyze the VASP calculations.[40] For each material, the crystal structure was obtained from the literature and reduced to the primitive cell. In cases where the reported crystal structure contained partial atomic site disorder, an ordered approximation of the unit cell was used. k-point meshes with a density of 2000 points per Å^{-3} were used for all calculations. In the structural relaxations, the lowest energy unit cell shape was found using the conjugate-gradient algorithm, allowing ion positions to move within the cell and allowing the cell to deform and change volume. The relaxations were run iteratively until the volume change between subsequent relaxations was less than 2%. After each structure was fully converged, a final electronic optimization was performed while keeping the structure fixed. For each material, the first ferromagnetic structural relaxations were instantiated with magnetic moments of 3.0 μ_B on each transition metal ion. For all calculations, `custodian`[40] was used to automatically monitor jobs and resubmit those which failed due to common errors. From these calculations, various structural, energetic, and magnetic parameters were aggregated. The magnetic moment on each ion was approximated by the projection of the fully converged spin-polarized wavefunctions onto spherical harmonics within a Wigner-Seitz radius of each atom. The default Wigner-Seitz radii included with the VASP PAW psuedopotentials were used for this purpose.

Derivation of the magnetic deformation

The degree of lattice deformation has previously been employed to quantify changes in, or compare similar crystal structures.[41,42] Here we define the magnetic deformation, Σ_M as the degree of lattice deformation between the DFT-optimized nonmagnetic and magnetic unit cells. To calculate Σ_M, the transformation matrix, $\boldsymbol{P}$, between the magnetic and nonmagnetic relaxed structures is determined from $\boldsymbol{P} = \boldsymbol{A}_{NM}^{-1} \cdot \boldsymbol{A}_M$ Where $\boldsymbol{A}_{NM}$ and $\boldsymbol{A}_M$ are respectively the lattice parameters of the non-magnetic and magnetic relaxed unit cell. In general, $\boldsymbol{P}$ may contain a rotational component, which does not contribute to deformation of the lattice. To remove this component, the Lagrangian finite strain tensor, $\boldsymbol{\eta}$, is calculated from $\boldsymbol{P}$:

$$\boldsymbol{\eta} = \frac{1}{2}(\boldsymbol{P}^T\boldsymbol{P} - \boldsymbol{I}) \tag{3}$$

The degree of lattice deformation is the root mean square of the eigenvalues of $\boldsymbol{\eta}$. Here, we express the magnetic deformation as a percentage:

$$\Sigma_M = \frac{1}{3}(\eta_1^2 + \eta_2^2 + \eta_3^2)^{1/2} \times 100 \tag{4}$$

A Python implementation of this calculation is provided in the Supporting Information.

Results and discussion

The experimental and computed properties for the 33 characterized magnetocalorics investigated in this study are shown in Table 1. For these materials, the experimental ΔS_M for applied field of both 2 T and 5 T correlate strongly with the calculated magnetic deformation, Σ_M (Figure 2 and Figure 3). In particular, the "giant" magnetocaloric effect materials in the database (MnAs and Fe_2P-based materials) are clearly separated from all other materials by their large values of lattice deformation ($\Sigma_M > 3\,\%$). These materials

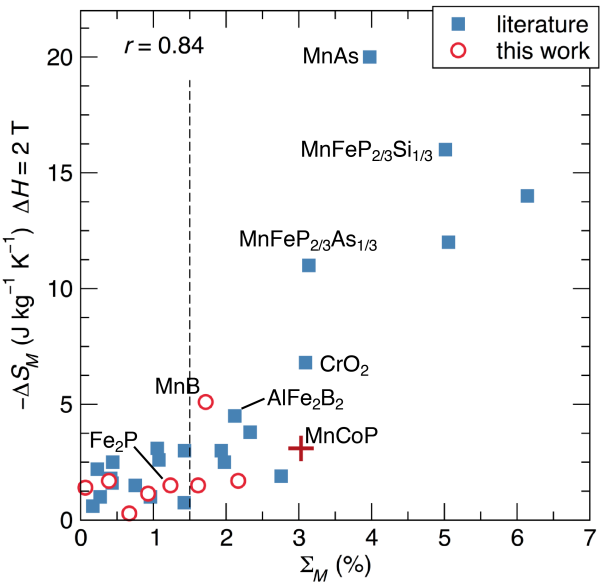

Figure 2: Comparison of the magnetic deformation, Σ_M and experimental maximum isothermal entropy change upon application of a 2 T magnetic field. The ΔS_M measurements include those obtained from previous studies and new measurements presented in this contribution. MnCoP, which was synthesized and measured after using Σ_M to screen candidate materials, is shown as a red plus. Pearson's r is indicated in the top left.

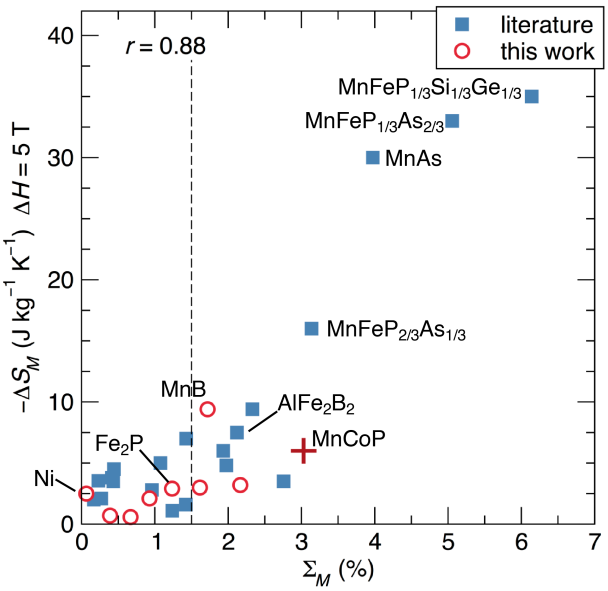

Figure 3: Comparison of Σ_M and maximum isothermal entropy change upon application of a 5 T magnetic field. Pearson's r is indicated in the top left.

Table 1: Selected experimental and calculated data for the magnetocalorics investigated in this study. The Curie temperature (T_C) and peak isothermal entropy change (ΔS_M) columns represent experimental results, either aggregated from literature (top section) or from new magnetic measurements in this study (bottom section). The magnetic deformation (Σ_M), saturation magnetization (M_S), percentage volume difference between the magnetic unit cell and the nonmangetic unit cell (ΔV_M), and density (ρ) are from DFT calculations performed in the present study. In each case, the ΔS_M is for the ferromagnetic to paramagnetic transition. MnB has also been measured by Fries et al.[64]

	T_C	ΔS_M (J kg^{-1} K^{-1})		ref.	Σ_M	M_S	ΔV_M	ρ
	(K)	$H = 2$ T	$H = 5$ T		(%)	(emu/g)	(%)	(g/cm^3)
MnAs	318	−20	−30	43	3.97	121.5	13.2	6.78
$MnFeP_{2/3}Si_{1/3}$	250	−16		44	5.02	171.1	7.10	6.67
$MnFeGe_{1/3}P_{1/3}Si_{1/3}$	275	−14	−35	45	6.14	154.7	5.80	7.13
$MnFeP_{1/3}As_{2/3}$	325	−12	−33	46	5.06	141.7	6.63	7.65
$MnFeP_{2/3}As_{1/3}$	225	−11	−16	46	3.14	146.0	7.10	7.22
CrO_2	396	−6.8		47	3.09	133.0	3.90	4.83
$AlFe_2B_2$	275	−4.5	−7.5	48	2.12	92.3	1.77	5.85
Mn_5Ge_3	300	−3.8	−9.4	49	2.33	152.5	11.3	7.49
Fe_3C	475	−3.1		50	1.05	170.2	5.53	7.94
$LaMnO_3$	300	−3	−7	51	1.43	71.2	7.42	6.55
MnCoGe	235	−3	−6	52	1.93	90.7	4.67	8.44
Mn_5PB_2	302	−2.6	−5	53	1.08	138.0	4.03	7.01
Y_2Fe_{17}	300	−2.5	−4.8	54	1.98	187.3	10.4	7.43
Mn_3GaC	250	−2.5	−4.5	55	0.44	95.0	2.31	7.40
MnSi	31	−2.2	−3.55	56	0.23	66.9	1.20	5.99
Mn_3Sn_2	280	−1.9	−3.5	57	2.76	107.3	8.15	7.91
MnP	290	−1.8	−3.8	58	0.41	46.9	1.22	6.17
Mn_3AlC	288	−1.6	−3.5	59	0.43	107.0	2.26	6.17
$MnNi_2Ga$	329	−1.5		60	0.75	93.7	3.93	8.26
Fe_5Si_3	373	−1	−2.8	49	0.96	111.7	3.13	6.70
La_2MnNiO_6	280	−1	−2.1	61	0.27	57.2	1.40	7.00
MnFeGe	235	−0.75	−1.6	52	1.42	83.8	3.68	8.36
$SrRuO_3$	160	−0.6	−2	62	0.17	47.3	0.84	6.31
Fe_3GeTe_2	225		−1.1	63	1.24	70.8	6.12	7.00
Ni	627	−1.4	−2.6	this work	0.07	55.6	0.34	9.03
Fe_2P	223	−1.5	−2.9	—*do.*—	1.23	116.7	3.64	7.15
MnB	571	−5.1	−9.4	—*do.*—	1.72	155.1	3.64	6.58
FeB	573	−1.7	−3.2	—*do.*—	2.17	96.6	1.52	7.00
MnNiSb	765	−1.5	−3.0	—*do.*—	1.61	94.9	8.50	7.60
$MnNi_2Sn$	350	−1.2	−2.1	—*do.*—	0.93	80.0	4.85	8.74
$FeRu_2Sn$	545	−0.3	−0.6	—*do.*—	0.67	61.7	3.49	10.4
$MnFe_2Si$	250	−0.6	−1.6	—*do.*—	0.39	86.1	2.03	7.46
MnCoP	583	−3.1	−6.0	—*do.*—	3.03	114.9	5.53	7.13

have discontinuous unit cell changes at their first-order magnetic phase transition, and Σ_M appears to capture this behavior. Interestingly, ΔS_M also correlates with Σ_M for the other materials in the dataset, which are not believed to have discontinuous magnetostructural transitions. This correlation appears to hold quite well across the full dataset, which spans a large range of structure types, magnetic exchange mechanisms, and elemental compositions. It is important to note that the correlation is not perfect, and a low value of Σ_M does not guarantee a low ΔS_M. However, the correlation does suggest that materials with higher values of Σ_M are much more likely to show high ΔS_M than materials with lower values of Σ_M. $\Sigma_M = 1.5$ % serves as a good cutoff: the compounds with $\Sigma_M >$1.5 are all remarkable magnetocalorics. Based on these results, we propose that Σ_M can be used as a screening parameter to identify compounds for experimental study.

The actual meaning of Σ_M is subtle. For the case of the Fe_2P-type materials in this dataset ($MnFeP_{2/3}Si_{1/3}$, $MnFeP_{1/3}Si_{1/3}Ge_{1/3}$, $MnFeP_{1/3}As_{2/3}$, and $MnFeP_{2/3}As_{1/3}$), the relaxed magnetic and nonmagnetic unit cell shapes qualitatively mirror the differences seen in the ferromagnetic and paramagnetic structures of these materials. Specifically, the relaxed magnetic unit cell has a larger hexagonal c axis and smaller a axis than the relaxed nonmagnetic cell, much like the experimental structural transition observed at the ferromagnetic to paramagnetic transition.[65] However, for most of the materials studied, there is no discontinuous structure change, and yet Σ_M is nonzero. Formally, Σ_M is indicating differences in equilibrium structure at 0 K between a material in a nonmagnetic state and in a ferromagnetic state. This 0 K nonmagnetic state is a poor representation of the high-temperature paramagnetic states, which has dynamically disordered moments. Therefore, it is best to describe Σ_M as an indication of the degree to which structural and magnetic degrees of freedom are coupled in a material, similar to magnetovolume coupling terms in the Bean and Rodbell model, which has been quite successful in analyzing magnetocalorics.[18,66] The strong correlation of ΔS_M with Σ_M highlights the importance of magnetostructural coupling in first order materials, but also indicates that magnetostruc-

tural coupling is important for strong magnetocaloric performance in materials displaying second-order magnetic transitions.

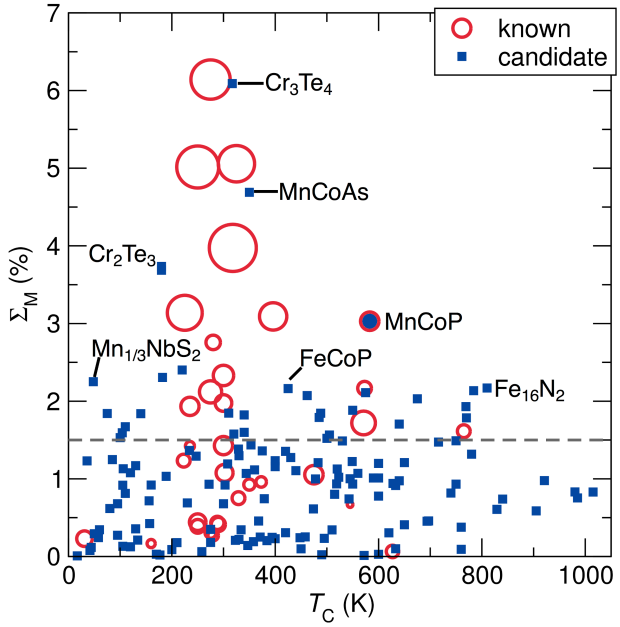

Figure 4: Σ_M *vs.* T_C for the known magnetocalorics and the candidate ferromagnetic materials. For the known magnetocalorics, the area of the circle is proportional to the material's peak ΔS_M with an applied field of 2 T. The grey line indicates $\Sigma_M = 1.5$; candidates above this line are predicted to show large ΔS_M. MnCoP, a candidate material with $\Sigma = 3.03\%$ which we have synthesized and measured, is shown with area proportional to its ΔS_M.[67–126]

The major advantages of Σ_M as a screening parameter is that it is computationally inexpensive and entirely material agnostic. Where more rigorous *ab initio* descriptions of exchange-volume coupling or magnetic entropy require detailed knowledge of a system, including the nature of the magnetic moments, the magnetic exchange mechanism, and the nature of the phase transition, Σ_M can be rapidly calculated for any material given only an ordered unit cell and no additional human input. Figure 4 shows Σ_M calculated for all 167 materials in this study, including the 134 that have not yet been studied for magnetocaloric effect, plotted against the experimental T_C. Thirty ferromagnets with $\Sigma_M > 1.5$ are identified and listed in Table 2. Based on the correlations observed in known magnetocalorics, these materials are likely to show strong magnetocaloric effect and are therefore

Table 2: Ferromagnetic compounds with large values of magnetic deformation, Σ_M (>1.5), indicating potential for good magnetocaloric properties. For each material, T_C is the experimental magnetic transition temperature (found in given reference). Σ_M and saturation magnetization (M_S) are the result of DFT calculations. The complete list of candidate compounds and calculated parameters can be found in the Supporting Information.

	T_C (K)	ref.	Σ_M (%)	M_S (emu/g)
Cr_3Te_4	317	67	6.09	83.7
MnCoAs	350	68	4.69	91.7
Cr_2Te_3	180	69	3.73	69.3
MnCoP	583	127	3.03	114.9
MnPtGa	220	70	2.40	65.5
CrNiAs	182	71	2.31	90.0
$MnNb_3S_6$	48	72	2.25	45.0
$Fe_{16}N_2$	810	73	2.17	213.4
FeCoP	425	68	2.16	78.0
Fe_5SiB_2	784	74	2.14	147.2
Fe_3Pd	575	75	2.11	168.8
Fe_3Pt	462	76	2.07	127.8
Fe_4CoSiB_2	675	77	2.03	117.9
Fe_4N	769	73	1.93	232.0
Fe_3N	550	78	1.88	187.8
$MnGa_2Sb_2$	310	79	1.85	34.7
Fe_2CoN	488	80	1.84	155.4
$MnTa_4S_8$	75	81	1.84	21.7
CrNiP	140	68	1.84	104.3
$MnGeAs_2$	340	82	1.82	83.6
$Fe_{23}Y_6$	485	83	1.79	152.8
Fe_4MnSiB_2	770	77	1.79	141.5
Fe_3Ge	640	84	1.70	147.8
Ba_2MnReO_6	110	85	1.67	35.8
$MnGe_4$	340	86	1.60	25.2
$Sr_3Ru_2O_7$	104	87	1.59	39.7
$MnGeP_2$	320	82	1.58	98.9
Fe_3RhN	505	88	1.56	168.9
$MnNb_4S_8$	100	81	1.53	29.7
MnPdSb	500	89	1.52	66.3

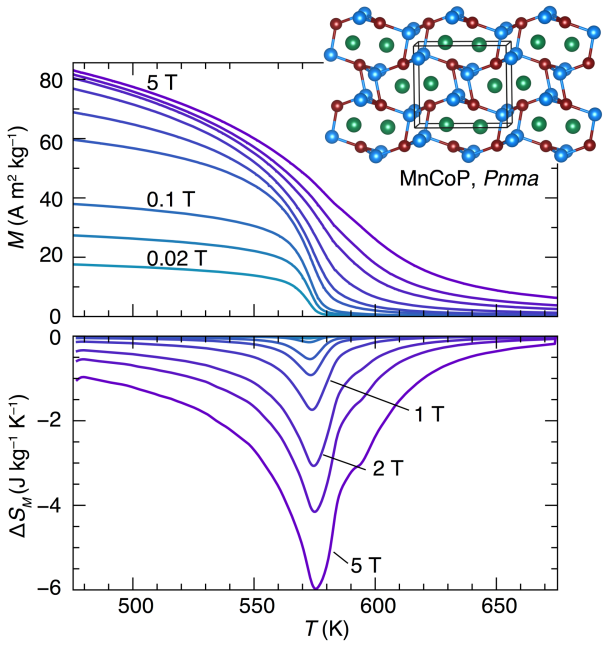

Figure 5: Magnetocaloric characterization of MnCoP, which shows a high Σ_M of 3.03%. Top: Magnetization *vs.* temperature at different magnetic fields. Bottom: ΔS_M, calculated from equation 2. The fields are 0.02 T, 0.05 T, 0.1 T, 0.3 T, 0.5 T, 1.0 T, 2.0 T, 3.0 T, and 5.0 T.

excellent candidates for experimental study.

We report here a first experimental verification of these predictions. MnCoP, an orthorhombic material with the TiNiSi structure ($Pnma$),[127] has $\Sigma_M = 3.03$ and is therefore expected to have strong ΔS_M near its Curie temperature of 583 K. We prepared this compound and measured its isothermal entropy change, as shown in Figure 5. MnCoP shows a maximum ΔS_M of 3.1 $\mathrm{kg^{-1}\,K^{-1}}$ for an applied field of 2 T and 6.0 $\mathrm{J\,kg^{-1}\,K^{-1}}$ for an applied field of 5 T. As shown in Figure 2 and Figure 3, these values fit well into the observed correlation between ΔS_M and Σ_M.

Currently, the most commonly used parameter in the search for new magnetocalorics is the saturation magnetization, M_S. Within systems, including some first order systems, the magnitude of ΔS_M is found to scale with M_S and looking for high magnetization compounds has often been a design principal in searching for new magnetocalorics.[128–130] The theoretical M_S of each of the materials in this dataset is easily calculated from the

magnetic DFT calculations. Surprisingly, despite the widespread acceptance of M_S as a key determiner of ΔS_M, the data shows poor correlation between M_S and ΔS_M. This can be seen in Figure 6, which is a visualization of the cross-correlation matrix for the properties investigated in this study. MnAs and the Fe_2P-based "giant" magnetocalorics show larger ΔS_M than Gd, despite having lower M_S. For the giant magnetocaloric effect materials, the failure of M_S as a predictor of ΔS_M can be understood as arising from the dominant role that the first-order magnetostructural transition plays in determining the entropy change. However, even for second order materials with no known discontinuous structural transition at the Curie temperature, deviation is expected. Using the Arrott-Noakes equation of state[131] for a second order magnetic transition and making the mean field approximation gives the following:[17]

$$\Delta S_M(H_1) = -\frac{1}{2}a\big[M(H_1) - M(0)\big] \tag{5}$$

Where the maximum entropy change upon isothermal application of a field H_1 is determined by a, a phenomenological parameter dependent on the critical exponents. $\big[M(H_1) - M(0)\big]$ is the difference between the magnetization under a field of H_1 and the spontaneous magnetization. Therefore, while large M_S provides the potential for large $\big[M(H_1) - M(0)\big]$, the value of $\Delta S_M(H_1)$ will ultimately depend heavily on the critical exponents and field-dependence of the magnetization curves.

The surprisingly poor correlation between calculated M_S and experimental ΔS_M can therefore be explained in both in materials displaying first- and second-order magnetic transitions. In both cases, the possible entropy change of the spin system upon magnetization is determined by the M_S, but the portion of that total change that can be caused by a finite magnetic field (*e.g.* 2 T or 5 T) is limited by other material properties that are not captured in a calculation of M_S.

Analysis of aggregated materials data has become an important and insightful way

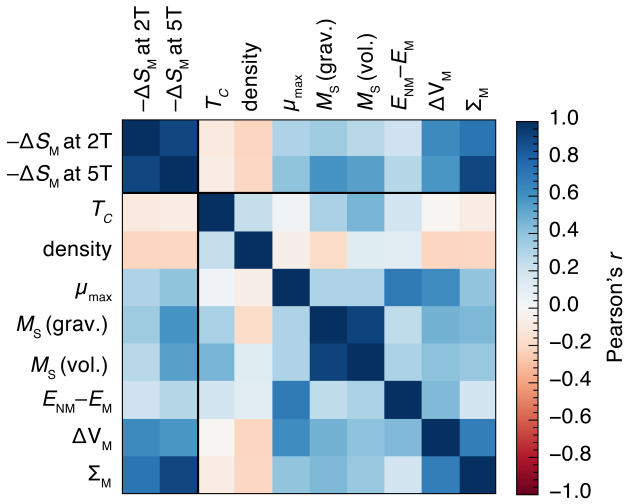

Figure 6: Visualization of the cross-correlation matrix for experimental (ΔS_M and T_C) and computed properties (all others). $\mu_{\max}$ is the maximum localized on any ion in the compound, and $E_{NM} - E_M$ is the energy difference between the structure calculated without and with spin-polarization, in eV/atom. For each square, the color represents Pearson's r, which ranges from -1 (perfect negative correlation) to $+1$ (perfect positive correlation) through 0 (no correlation). Correlations involving ΔS_M use the 33 magnetocaloric materials (Table 1), while all other correlations use the full dataset of 167 materials (Table 2, Supporting Information Table S2).

of understanding physical phenomena, especially as large databases of experimental and computational data have been established.[132–139] Statistical analysis, interactive visualization, and machine learning allow for new and insightful ways of understanding materials behavior and guiding research efforts. The experimental and computed data in this study, provided in full in the Supporting Information, afford opportunities for this type of analysis. For example, Figure 6 contains a cross-correlation analysis of the parameters investigated in this study, including measured ΔS_M and T_C and several properties extracted from the DFT calculations. This analysis shows that ΔS_M for applied fields of both 2 T and 5 T is more strongly correlated with Σ_M than with any other calculated property investigated. The percentage volume change between the nonmagnetic unit cell and the magnetic unit cell also shows some correlation with ΔS_M, although less than the magnetic deformation. While the cell volume captures some of the structural differences that arise between the magnetic unit cell and nonmagnetic unit cell, it fails to account for cases where significant

unit cell shape changes occur without large changes in cell volume. These sort of structural transitions can be important in magnetocaloric materials, for example in the case of the Fe_2P-type compounds discussed earlier. Numerous other correlations are found between various parameters. For example, $E_{\mathrm{NM}} - E_{\mathrm{M}}$, which can be viewed as the energy benefit of a material becoming magnetic, is much more strongly related to the maximum ionic moment size $\mu_{\max}$ than to any other parameter, including the overall magnetization M_S. This suggests that a large ionic moment is a sign of a highly stable magnetic ground state. Interestingly, this analysis also shows that none of the investigated parameters correlates particularly well with T_C. As T_C is an important parameter in screening magnets for a variety of applications, including magnetocalorics, it will be valuable to investigate simple and general computational methods of predicting T_C.

Conclusion

This contribution introduces a simple computational proxy for the screening of magnetic materials for magnetocaloric performance, Σ_M, the magnetic deformation. This proxy is validated using ΔS_M values from reported magnetocalorics and new ΔS_M measurements. Based on application of this proxy to ferromagnets that have not yet been measured for ΔS_M, we propose 30 likely candidates for strong magnetocaloric performance. The calculation of Σ_M requires no knowledge of a material beyond it's crystal structure, so the method is easily applied to a large number of compounds. While this study has restricted screening to known ferromagnets with relatively simple unit cells and no rare earth elements, the proxy is quite general and could be used across a large variety of systems. For example, by combining this proxy with phase stability analysis,[134] this proxy could be applied to screen large numbers of hypothetical materials that are expected to be thermodynamically stable but have not yet been experimentally investigated. Alternatively, this proxy can be used to screen compositions within a single system to suggest compositions

with optimal properties. Furthermore, as many known magnetocaloric materials have magnetic transitions other than the transition from paramagnetic to ferromagnetic states, it would be profitable to expand this proxy to a wider range of materials by comparing the structures of materials with other kinds of magnetic orderings, such as antiferromagnets and ferrimagnets.

Acknowledgement

This work was supported by the National Science Foundation through DMR-1121053. J.D.B. is supported by the National Science Foundation Graduate Research Fellowship Program under Grant No. 1650114. We thank Dr. Jason Douglas for providing a sample of $FeRu_2Sn$. This work made use of the shared experimental facilities of the Materials Research Laboratory, supported by the NSF MRSEC Program (DMR-1121053), and the Center for Scientific Computing at UCSB, supported by NSF MRSEC (DMR-1121053), NSF CNS-0960316 and Hewlett Packard. The Materials Research Laboratory is a member of the NSF-supported Materials Research Facilities Network. Use of the Advanced Photon Source at Argonne National Laboratory was supported by the U. S. Department of Energy, Office of Science, Office of Basic Energy Sciences, under Contract No. DE-AC02-06CH11357.

References

(1) Giauque, W. F.; MacDougall, D. P. Attainment of temperatures below 1° absolute by demagnetization of $Gd_2(SO_4)_3 \cdot 8\ H_2O$. *Phys. Rev.* **1933**, *43*, 768–768.

(2) Franco, V.; Blázquez, J.; Ingale, B.; Conde, A. The magnetocaloric effect and magnetic refrigeration near room temperature: materials and models. *Annu. Rev. Mater. Res.* **2012**, *42*, 305–342.

(3) Brown, G. V. Magnetic heat pumping near room temperature. *J. Appl. Phys.* **1976**, *47*, 3673.

(4) Zimm, C.; Jastrab, A.; Sternberg, A.; Pecharsky, V.; Gschneidner, K.; Osborne, M.; Anderson, I. *Adv. Cryog. Eng.*; Springer US: Boston, MA, 1998; pp 1759–1766.

(5) Takeuchi, I.; Sandeman, K. Solid-state cooling with caloric materials. *Phys. Today* **2015**, *68*, 48–54.

(6) Pecharsky, V. K.; Cui, J.; Johnson, D. D. (Magneto)caloric refrigeration: Is there light at the end of the tunnel? *Philos. Trans. R. Soc., A* **2016**, *374*, 20150305.

(7) Cam Thanh, D. T.; Brück, E.; Trung, N. T.; Klaasse, J. C. P.; Buschow, K. H. J.; Ou, Z. Q.; Tegus, O.; Caron, L. Structure, magnetism, and magnetocaloric properties of $MnFeP_{1-x}Si_x$ compounds. *J. Appl. Phys.* **2008**, *103*, 07B318.

(8) Boeije, M. F. J.; Roy, P.; Guillou, F.; Yibole, H.; Miao, X. F.; Caron, L.; Banerjee, D.; van Dijk, N. H.; de Groot, R. A.; Brück, E. Efficient Room-Temperature Cooling with Magnets. *Chem. Mater.* **2016**, *28*, 4901–4905.

(9) Hu, F.-X.; Shen, B.-G.; Sun, J.-R.; Cheng, Z.-H.; Rao, G.-H.; Zhang, X.-X. Influence of negative lattice expansion and metamagnetic transition on magnetic entropy change in the compound $LaFe_{11.4}Si_{1.6}$. *Appl. Phys. Lett.* **2001**, *78*, 3675–3677.

(10) Krenke, T.; Duman, E.; Acet, M.; Wassermann, E. F.; Moya, X.; Mañosa, L.; Planes, A. Inverse magnetocaloric effect in ferromagnetic NiMnSn alloys. *Nat. Mater.* **2005**, *4*, 450–454.

(11) Liu, J.; Gottschall, T.; Skokov, K. P.; Moore, J. D.; Gutfleisch, O. Giant magnetocaloric effect driven by structural transitions. *Nat. Mater.* **2012**, *11*, 620–626.

(12) Pecharsky, V. K.; Gschneidner, K. A. Advanced magnetocaloric materials: What does the future hold? *Int. J. Refrig.* **2006**, *29*, 1239–1249.

(13) Kitanovski, A.; Plaznik, U.; Tomc, U.; Poredoš, A. Present and future caloric refrigeration and heat-pump technologies. *Int. J. Refrig.* **2015**, *57*, 288–298.

(14) Christiaanse, T.; Brück, E. Proof-of-concept static thermomagnetic generator experimental device. *Metall. Mater. Trans. E* **2014**, *1*, 36–40.

(15) Elliott, J. F.; Legvold, S.; Spedding, F. H. Some magnetic properties of gadolinium metal. *Phys. Rev.* **1953**, *91*, 28–30.

(16) Dan'kov, S.; Tishin, a.; Pecharsky, V.; Gschneidner, K. Magnetic phase transitions and the magnetothermal properties of gadolinium. *Phys. Rev. B* **1998**, *57*, 3478–3490.

(17) Franco, V.; Conde, A. Scaling laws for the magnetocaloric effect in second order phase transitions: From physics to applications for the characterization of materials. *Int. J. Refrig.* **2010**, *33*, 465–473.

(18) Belo, J. H.; Amaral, J. S.; Pereira, A. M.; Amaral, V. S.; Araújo, J. P. On the Curie temperature dependency of the magnetocaloric effect. *Appl. Phys. Lett.* **2012**, *100*, 242407.

(19) Pecharsky, V. K.; Gschneidner, Jr., K. A. Giant magnetocaloric effect in $Gd_5(Si,Ge)_2$. *Phys. Rev. Lett.* **1997**, *78*, 4494–4497.

(20) Magen, C.; Arnold, Z.; Morellon, L.; Skorokhod, Y.; Algarabel, P. A.; Ibarra, M. R.; Kamarad, J. Pressure-induced three-dimensional ferromagnetic correlations in the giant magnetocaloric compound Gd_5Ge_4. *Phys. Rev. Lett.* **2003**, *91*, 207202.

(21) Choe, W.; Miller, G. J.; Meyers, J.; Chumbley, S.; Pecharsky, A. O. Nanoscale zippers in the crystalline Solid. Structural variations in the giant magnetocaloric material $Gd_5Si_{1.5}Ge_{2.5}$. *Chem. Mater.* **2003**, *15*, 1413–1419.

(22) Łażewski, l. J.; Piekarz, P.; Toboła, J.; Wiendlocha, B.; Jochym, P. T.; Sternik, M.; Parlinski, K. Phonon mechanism of the magnetostructural phase transition in MnAs. *Phys. Rev. Lett.* **2010**, *104*, 147205.

(23) Jain, A.; Ong, S. P.; Hautier, G.; Chen, W.; Richards, W. D.; Dacek, S.; Cholia, S.; Gunter, D.; Skinner, D.; Ceder, G.; Persson, K. A. Commentary: The Materials Project: A materials genome approach to accelerating materials innovation. *APL Mater.* **2013**, *1*, 011002.

(24) Saal, J. E.; Kirklin, S.; Aykol, M.; Meredig, B.; Wolverton, C. Materials design and discovery with high-throughput density functional theory: The Open Quantum Materials Database (OQMD). *JOM* **2013**, *65*, 1501–1509.

(25) Curtarolo, S.; Setyawan, W.; Wang, S.; Xue, J.; Yang, K.; Taylor, R. H.; Nelson, L. J.; Hart, G. L.; Sanvito, S.; Buongiorno-Nardelli, M.; Mingo, N.; Levy, O. AFLOWLIB.ORG: A distributed materials properties repository from high-throughput *ab initio* calculations. *Comput. Mater. Sci.* **2012**, *58*, 227–235.

(26) Yan, J.; Gorai, P.; Ortiz, B.; Miller, S.; Barnett, S. A.; Mason, T.; Stevanović, V.; Toberer, E. S. Material descriptors for predicting thermoelectric performance. *Energy Environ. Sci.* **2015**, *8*, 983–994.

(27) Brgoch, J.; DenBaars, S. P.; Seshadri, R. Proxies from *ab initio* calculations for screening efficient Ce^{3+} phosphor hosts. *J. Phys. Chem. C* **2013**, *117*, 17955–17959.

(28) Adams, S.; Rao, R. P. High power lithium ion battery materials by computational design. *Phys. status solidi* **2011**, *208*, 1746–1753.

(29) Melot, B. C.; Scanlon, D. O.; Reynaud, M.; Rousse, G.; Chotard, J.-N.; Henry, M.; Tarascon, J.-M. Chemical and structural indicators for large redox potentials in Fe-based positive electrode materials. *ACS Appl. Mater. & Interfaces* **2014**, *6*, 10832–10839.

(30) Rong, Z.; Malik, R.; Canepa, P.; Sai Gautam, G.; Liu, M.; Jain, A.; Persson, K.; Ceder, G. Materials design rules for multivalent ion mobility in intercalation structures. *Chem. Mater.* **2015**, *27*, 6016–6021.

(31) Miao, X. F.; Caron, L.; Gercsi, Z.; Daoud-Aladine, A.; van Dijk, N. H.; Brück, E. Thermal-history dependent magnetoelastic transition in $(Mn,Fe)_2(P,Si)$ *Appl. Phys. Lett.* **2015**, *107*, 042403 .

(32) Douglas, J. E.; Levin, E. E.; Pollock, T. M.; Castillo, J. C.; Adler, P.; Felser, C.; Krämer, S.; Page, K. L.; Seshadri, R. Magnetic hardening and antiferromagnetic/ferromagnetic phase coexistence in $Mn_{1-x}Fe_xRu_2Sn$ Heusler solid solutions. *Phys. Rev. B* **2016**, *94*, 094412.

(33) Larson, A. C.; Von Dreele, R. B. General Structure Analysis System (GSAS). *Los Alamos Natl. Lab. Rep. LAUR* **2000**, , 86–748 .

(34) Toby, B. H; EXPGUI, a graphical user interface for GSAS *J. Appl. Crystallogr.* **2001**, *34*, 210–213 .

(35) Momma, K.; Izumi, F.; VESTA 3 for three-dimensional visualization of crystal, volumetric and morphology data *J. Appl. Crystallogr.* **2011**, *44*, 1272–1276 .

(36) Kresse, G.; Furthmüller, J. Efficient iterative schemes for ab initio total-energy calculations using a plane-wave basis set. *Phys. Rev. B* **1996**, *54*, 11169–11186.

(37) Blöchl, P. E. Projector augmented-wave method. *Phys. Rev. B* **1994**, *50*, 17953–17979.

(38) Kresse, G.; Joubert, D. From ultrasoft pseudopotentials to the projector augmented-wave method. *Phys. Rev. B* **1999**, *59*, 1758–1775.

(39) Perdew, J. P.; Burke, K.; Ernzerhof, M. Generalized gradient approximation made simple. *Phys. Rev. Lett.* **1996**, *77*, 3865–3868.

(40) Ong, S. P.; Richards, W. D.; Jain, A.; Hautier, G.; Kocher, M.; Cholia, S.; Gunter, D.; Chevrier, V. L.; Persson, K. A.; Ceder, G. Python Materials Genomics (pymatgen): A robust, open-source python library for materials analysis. *Comput. Mater. Sci.* **2013**, *68*, 314–319.

(41) Catti, M. Calculation of elastic constants by the method of crystal static deformation. *Acta Crystallogr., Sect. A Found. Crystallogr.* **1985**, *41*, 494–500.

(42) de la Flor, G.; Orobengoa, D.; Tasci, E.; Perez-Mato, J. M.; Aroyo, M. I. Comparison of structures applying the tools available at the Bilbao Crystallographic Server. *J. Appl. Crystallogr.* **2016**, *49*, 653–664.

(43) Wada, H.; Tanabe, Y. Giant magnetocaloric effect of $MnAs_{1-x}Sb_x$. *Appl. Phys. Lett.* **2001**, *79*, 3302.

(44) Katagiri, K.; Nakamura, K.; Wada, H. Magnetocaloric properties and magnetic refrigerant capacity of $MnFeP_{1-x}Si_x$. *J. Alloys Compd.* 286–290.

(45) Thanh, D. T. C.; Brück, E.; Tegus, O.; J. C. P., K.; Gortenmulder, T. J.; Buschow, K. H. J. Magnetocaloric effect in MnFe(P,Si,Ge) compounds. *J. Appl. Phys.* **2006**, *99*, 08Q107.

(46) Tegus, O.; Brück, E.; Zhang, L.; Dagula,; Buschow, K. H. J.; de Boer, F. R. Magnetic-phase transitions and magnetocaloric effects. *Physica B: Condensed Matter* **2002**, *319*, 174–192.

(47) Zhang, X.; Chen, Y.; Lü, L.; Li, Z. A potential oxide for magnetic refrigeration application: CrO_2 particles. *J. Phys.: Condensed Matter* **2006**, *18*, L559–L566.

(48) Tan, X.; Chai, P.; Thompson, C. M.; Shatruk, M. Magnetocaloric effect in $AlFe_2B_2$: toward Magnetic refrigerants from earth-abundant elements. *J. Am. Chem. Soc.* **2013**, *135*, 9553–9557.

(49) Songlin; Dagula; Tegus, O.; Brück, E.; Klaasse, J. C. P.; de Boer, F. R.; Buschow, K. H. J. Magnetic phase transition and magnetocaloric effect in $Mn_{5-x}Fe_xSi_3$. *J. Alloys Compd.* **2002**, *334*, 249–252.

(50) Kaeswurm, B.; Friemert, K.; Gürsoy, M.; Skokov, K. P.; Gutfleisch, O. Direct measurement of the magnetocaloric effect in cementite. *J. Magn. Magn. Mater.* **2016**, *410*, 105–108.

(51) Phan, M.-H.; Yu, S.-C. Review of the magnetocaloric effect in manganite materials. *J. Magn. Magn. Mater.* **2007**, *308*, 325–340.

(52) Lin, S.; Tegus, O.; Brück, E.; Dagula, W.; Gortenmulder, T.; Buschow, K. Structural and magnetic properties of $MnFe_{1-x}Co_xGe$ Compounds. *IEEE Trans. Magn.* **2006**, *42*, 3776–3778.

(53) Xie, Z. G.; Geng, D. Y.; Zhang, Z. D. Reversible room-temperature magnetocaloric effect in Mn_5PB_2. *Appl. Phys. Lett.* **2010**, *97*, 202504.

(54) Llamazares, J. S.; Álvarez-Alonso, P.; Sánchez-Valdés, C.; Ibarra-Gaytán, P. J.; Blanco, J. A.; Gorria, P. Investigating the magnetic entropy change in single-phase Y_2Fe_{17} melt-spun ribbons. *Curr. Appl. Phys.* **2016**, *16*, 963–968.

(55) Tong, P.; Wang, B.-S.; Sun, Y.-P. Mn-based antiperovskite functional materials: Review of research. *Chin. Phys. B.* **2013**, *22*, 067501.

(56) Arora, P.; Chattopadhyay, M. K.; Roy, S. B. Magnetocaloric effect in MnSi. *Appl. Phys. Lett.* **2007**, *91*, 062508.

(57) Recour, Q.; Mazet, T.; Malaman, B. Magnetocaloric properties of Mn_3Sn_2 from heat capacity measurements. *J. Appl. Phys.* **2009**, *105*, 033905.

(58) Booth, R. A.; Majetich, S. A. Crystallographic orientation and the magnetocaloric effect in MnP. *J. Appl. Phys.* **2009**, *105*, 07A926.

(59) Tong, P.; Wang, B.-S.; Sun, Y.-P. Mn-based antiperovskite functional materials: Review of research. *Chin. Phys. B.* **2013**, *22*, 067501.

(60) Tegus, O.; Brück, E.; Zhang, L.; Dagula,; Buschow, K. H. J.; de Boer, F. R. Magnetic-phase transitions and magnetocaloric effects. *Physica B: Condensed Matter* **2002**, *319*, 174–192.

(61) Balli, M.; Fournier, P.; Jandl, S.; Gospodinov, M. M. A study of the phase transition and magnetocaloric effect in multiferroic La_2MnNiO_6 single crystals. *J. Appl. Phys.* **2014**, *115*, 173904.

(62) Zhang, X.-Y.; Chen, Y.; Li, Z.-Y. Magnetocaloric effect in 4d itinerant ferromagnet $SrRuO_3$. *J. Alloys Compd.* **2008**, *459*, 51–54.

(63) Verchenko, V. Y.; Tsirlin, A. A.; Sobolev, A. V.; Presniakov, I. A.; Shevelkov, A. V. Ferromagnetic order, strong magnetocrystalline anisotropy, and magnetocaloric effect in the layered telluride $Fe_{3-\delta}GeTe_2$. *Inorg. Chem.* **2015**, *54*, 8598–8607.

(64) Fries, M.; Gercsi, Z.; Ener, S.; Skokov, K. P.; Gutfleisch, O. Magnetic, magnetocaloric and structural properties of manganese based monoborides doped with iron and

cobalt − A candidate for thermomagnetic generators. *Acta Mater.* **2016**, *113*, 213–220.

(65) Dung, N. H.; Zhang, L.; Ou, Z. Q.; Bruck, E. From first-order magneto-elastic to magneto-structural transition in (Mn,Fe)$_{1.95}$P$_{0.50}$Si$_{0.50}$ compounds. *Appl. Phys. Lett.* **2011**, *99*, 092511.

(66) Bean, C. P.; Rodbell, D. S. Magnetic disorder as a first-order phase transformation. *Phys. Rev.* **1962**, *126*, 104–115.

(67) Akram, M.; Nazar, F. M. Magnetic properties of CrTe, $Cr_{23}Te_{24}$, Cr_7Te_8, Cr_5Te_6, and Cr_3Te_4 compounds. *J. Mater. Sci.* **1983**, *18*, 423–429.

(68) Nylund, M. A.; Roger, M. M. A.; Sénateur, J. P.; Fruchart, R. Evolution structurale des phosphures, arséniures et arséniophosphures M_2P, M_2As et M_2(P$_{1-x}$As$_x$). *J. Solid State Chem.* **1972**, *4*, 115–122.

(69) Yuzuri, M.; Kanomata, T.; Kaneko, T. The pressure effect on the Curie temperature and exchange striction of Cr_2S_3 and Cr_2Te_3. *J. Magn. Magn. Mater.* **1987**, *70*, 223–224.

(70) Buschow, K. H. J.; Mooij, D. B. D. Crystal structure and magnetic properties of PtMnGa and PtMnAl. *J. Less Common Met.* **1984**, *99*, 125–130.

(71) Bacmann, M.; Fruchart, D.; Koumina, A.; Wolfers, P. Low temperature magnetic structure of CrNiAs. *Mater. Sci. Forum* **2004**, *443-444*, 379–382.

(72) Hulliger, F.; Pobitschka, E. On the magnetic behavior of new 2H-NbS_2-type derivatives. *J. Solid State Chem.* **1970**, *1*, 117–119.

(73) Coey, J. M. D. *Magnetism and Magnetic Materials*; Magnetism and Magnetic Materials; Cambridge University Press, 2010.

(74) R, W.; Ericsson, T.; Häggström, L.; Andersson, Y. Magnetic properties of Fe_5SiB_2 and related compounds. *J. Phys. Colloq.* **1976**, *37*, C6–591–C6–593.

(75) Cui, J.; James, R. D. Study of Fe_3Pd and related alloys for ferromagnetic shape memory. *IEEE Trans. Magn.* **2001**, *37*, 2675–2677.

(76) Seeger, M.; Kronmüller, H. The magnetic phase transition in ordered and disordered ferromagnets. *J. Magn. Magn. Mater.* **1989**, *78*, 393–402.

(77) McGuire, M. A.; Parker, D. S. Magnetic and structural properties of ferromagnetic Fe_5PB_2 and Fe_5SiB_2 and effects of Co and Mn substitutions. *J. Appl. Phys.* **2015**, *118*, 163903.

(78) Gambino, R. J. Magnetic properties of the iron-group metal phosphides. *J. Appl. Phys.* **1967**, *38*, 1253.

(79) Sakakibara, W.; Hayashi, Y.; Takizawa, H. $MnGa_2Sb_2$, a new ferromagnetic compound synthesized under high pressure. *J. Ceram. Soc. Jpn.* **2009**, *117*, 72–75.

(80) Guo, K.; Rau, D.; Toffoletti, L.; Müller, C.; Burkhardt, U.; Schnelle, W.; Niewa, R.; Schwarz, U. Ternary metastable nitrides ϵ-Fe_2TMN (TM = Co, Ni): High-pressure, high-temperature synthesis, crystal structure, thermal stability, and magnetic properties. *Chem. Mater.* **2012**, *24*, 4600–4606.

(81) Ōnuki, Y.; Ina, K.; Hirai, T.; Komatsubara, T. Magnetic properties of intercalation compound: $Mn_{1/4}MX_2$. *J. Phys. Soc. Jpn.* **1986**, *55*, 347–356.

(82) Cho, S.; Choi, S.; Cha, G.-B.; Hong, S. C.; Kim, Y.; Freeman, A. J.; Ketterson, J. B.; Park, Y.; Park, H.-M. Synthesis of new pure ferromagnetic semiconductors: $MnGeP_2$ and $MnGeAs_2$. *Solid State Commun.* **2004**, *129*, 609–613.

(83) Buschow, K. H. J. Hydrogen absorption and its effect on the magnetic properties of rare-earth iron intermetallics. *Solid State Commun.* **1976**, *19*, 421–423.

(84) Drijver, J. W.; Sinnema, S. G.; van der Woude, F. Magnetic properties of hexagonal and cubic Fe_3Ge. *J. Phys. F.* **1976**, *6*, 2165–2177.

(85) Serrate, D.; Teresa, J. M. D.; Ibarra, M. R. Double perovskites with ferromagnetism above room temperature. *J. Phys.: Condensed Matter* **2006**, *19*, 023201.

(86) Takizawa, H.; Sato, T.; Endo, T.; Shimada, M. High pressure synthesis and electrical and magnetic properties of $MnGe_4$ and $CoGe_4$. *J. Solid State Chem.* **1990**, *88*, 384–390.

(87) Cao, G.; McCall, S.; Crow, J. E. Observation of itinerant ferromagnetism in layered $Sr_3Ru_2O_7$ single crystals. *Phys. Rev. B.* **1997**, *55*, R672–R675.

(88) Houben, A.; Müller, P.; von Appen, J.; Lueken, H.; Niewa, R.; Dronskowski, R. Synthesis, crystal structure, and magnetic properties of the semihard Itinerant Ferromagnet $RhFe_3N$. *Angew. Chem.* **2005**, *44*, 7212–7215.

(89) Endo, K. Magnetic studies of $C1_b$-Compounds CuMnSb, PdMnSb and Cu_{1-x}(Ni or Pd)$_x$MnSb. *J. Phys. Soc. Jpn.* **1970**, *29*, 643–649.

(90) Klemmer, T.; Hoydick, D.; Okumura, H.; Zhang, B.; Soffa, W. A. Magnetic hardening and coercivity mechanisms in $L1_0$ ordered FePd ferromagnets. *Scripta Metal. Mater.* **1995**, *33*, 1793–1805.

(91) Webster, P. J. Heusler alloys. *Contemp. Phys.* **1969**, *10*, 559–577.

(92) Grandjean, F.; Gerard, A. Study by Mossbauer spectroscopy of the series of perovskite carbides M_3M'C with M=Fe or Mn, and M'=Al, Ga, Ge, Zn, Sn. *J. Phys. F.* **1976**, *6*, 451–467.

(93) Miyatani, K.; Wada, Y.; Okamoto, F. Magnetic properties of single crystal chalcogenide spinels; $CuCr_2X_3Y$ (X = S, Se and Te, Y = Cl, Br and I) system. *J. Phys. Soc. Jpn.* **1968**, *25*, 369–372.

(94) Iga, A.; Tawara, Y. Magnetic properties of molybdenum- and wolfram-Modified Mn_3B_4. *J. Phys. Soc. Jpn.* **1968**, *24*, 28–35.

(95) Irkhin, V. Y.; Katsnel'son, M. I. Half-metallic ferromagnets. *Phys. Uspekhi* **1994**, *37*, 659–676.

(96) Nakatani, I.; Nosé, H.; Masumoto, K. Magnetic properties of $CuCr_2Se_4$ single crystals. *J. Phys. Chem. Solids* **1978**, *39*, 743–749.

(97) Menyuk, N. Ferromagnetism in $CdCr_2Se_4$ and $CdCr_2S_4$. *J. Appl. Phys.* **1966**, *37*, 1387.

(98) Shull, R. D.; Okamoto, H.; Beck, P. A. Transition from ferromagnetism to mictomagnetism in Fe-Al alloys. *Solid State Commun.* **1976**, *20*, 863–868.

(99) Wojtowicz, P. Semiconducting ferromagnetic spinels. *IEEE Trans. Magn.* **1969**, *5*, 840–848.

(100) Tsuzuki, A.; Sago, S.; Hirano, S. I.; Naka, S. High temperature and pressure preparation and properties of iron carbides Fe_7C_3 and Fe_3C. *J. Mater. Sci.* **1984**, *19*, 2513–2518.

(101) Mattern, N.; Zhang, W. X.; Roth, S.; Reuther, H.; Baehtz, C.; Richter, M. Structural and magnetic properties of non-stoichiometric Fe_2Zr. *J. Phys.: Condensed Matter* **2007**, *19*, 376202.

(102) Sankar, S. G.; Wallace, W. E. Magnetic properties of $ScFe_2$. AIP Conf. Proc. 1976.

(103) Chikazumi, S. *Physics of Ferromagnetism 2e*; Int. Ser. Monogr. Phys.; OUP Oxford, 2009.

(104) Zhang, Z.-D.; Kershaw, R.; Dwight, K.; Wold, A. Preparation and characterization of nickel substituted Fe_5C_2. *Mater. Res. Bull.* **1986**, *21*, 979–983.

(105) Buschow, K. H. J.; van Diepen, A. M. Effect of hydrogen absorption on the magnetic properties of YFe_2 and $GdFe_2$. *Solid State Commun.* **1976**, *19*, 79–81.

(106) Kanomata, T.; Kaneko, T.; Nakagawa, Y. Magnetic properties of the intermetallic compound Mn_3InC. *J. Solid State Chem.* **1992**, *96*, 451–454.

(107) Marei, S. A.; Craig, R. S.; Wallace, W. E.; Tsuchida, T. Magnetic characteristics of some Laves phase systems containing Fe and Mn. *J. Less Common Met.* **1967**, *13*, 391–398.

(108) Deka, B.; Kundu, A.; Ghosh, S.; Srinivasan, A. Experimental and *ab initio* studies on sub-lattice ordering and magnetism in $Co_2Fe(Ge_{1-x}Si_x)$ alloys. *J. Appl. Phys.* **2015**, *118*, 133906.

(109) Hayashi, N.; Yamamoto, T.; Kageyama, H.; Nishi, M.; Watanabe, Y.; Kawakami, T.; Matsushita, Y.; Fujimori, A.; Takano, M. $BaFeO_3$: A ferromagnetic iron oxide. *Angew. Chem.* **2011**, *50*, 12547–12550.

(110) Shinjo, T.; Nakamura, Y.; Shikazono, N. Magnetic study of Fe_3Si and Fe_5Si_3 by Mössbauer effect. *J. Phys. Soc. Jpn.* **1963**, *18*, 797–801.

(111) Cadeville, M. C.; Dahmani, C. E.; Kern, F. Magnetism and spatial order in Ni-Pt and Co-Pt alloys. *J. Magn. Magn. Mater.* **1986**, *54-57*, 1055–1056.

(112) Zhurakovskii, E. A.; Shashkina, T. B.; Kotlyar, V. I. X-ray absorption spectra of cobalt in ferromagnetic borides. *Soviet Phys. J.* **1970**, *13*, 14–17.

(113) Barón-González, A. J.; Frontera, C.; García-Muñoz, J. L.; Blasco, J.; Ritter, C. Cation order and structural transition in La_2MnCoO_6. *J. Phys.: Conf. Ser.* **2011**, *325*, 012007.

(114) Kübler, J.; Fecher, G. H.; Felser, C. Understanding the trend in the Curie temperatures of Co_2-based Heusler compounds: *Ab initio* calculations. *Phys. Rev. B* **2007**, *76*.

(115) Cadeville, M. C. Proprietes magnetiques des diborures de manganese et de chrome: MnB_2 et CrB_2. *J. Phys. Chem. Solids* **1966**, *27*, 667–670.

(116) Miyahara, S. Magnetic properties of FeS_2 and CoS_2. *J. Appl. Phys.* **1968**, *39*, 896.

(117) Jin, C. Q.; Zhou, J. S.; Goodenough, J. B.; Liu, Q. Q.; Zhao, J. G.; Yang, L. X.; Yu, Y.; Yu, R. C.; Katsura, T.; Shatskiy, A.; Ito, E. High-pressure synthesis of the cubic perovskite $BaRuO_3$ and evolution of ferromagnetism in $A\mathrm{RuO}_3$ (A = Ca, Sr, Ba) ruthenates. *Proc. Natl. Acad. Sci.* **2008**, *105*, 7115–7119.

(118) Wolcott, N. M.; Falge, R. L. Ferromagnetism of $CrBe_{12}$. *Phys. Rev.* **1968**, *171*, 591–595.

(119) Bainsla, L.; Suresh, K. G. Spin polarization studies in half-metallic $Co_2\mathrm{Ti}X$ (X = Ge and Sn) Heusler alloys. *Curr. Appl. Phys.* **2016**, *16*, 68–72.

(120) van Engen, P. G.; Buschow, K. H. J.; Erman, M. Magnetic properties and magneto-optical spectroscopy of Heusler alloys based on transition metals and Sn. *J. Magn. Magn. Mater.* **1983**, *30*, 374–382.

(121) Terada, M.; Endo, K.; Fujita, Y.; Kimura, R. Magnetic Properties of $C1_b$ Compounds; CoVSb, CoTiSb and NiTiSb. *J. Phys. Soc. Jpn.* **1972**, *32*, 91–94.

(122) Kouacou, M. A.; Pierre, J.; Skolozdra, R. V. Semiconductor-metal transition and the onset of itinerant ferromagnetism in the Heusler phases TiCoSn-TiCoSb. *J. Phys.: Condensed Matter* **1995**, *7*, 7373–7385.

(123) Pal, L.; Gupta, S.; Suresh, K. Structural and magnetic properties of $Co_2\mathrm{Ti}_{1-x}\mathrm{Fe}_x\mathrm{Al}$ ($0 \leq x \leq 0.5$) Alloys. AIP Conf. Proc. 2014; pp 1526–1528.

(124) Takahashi, Y. On the origin of the Curie-Weiss law of the magnetic susceptibility in itinerant electron ferromagnetism. *J. Phys. Soc. Jpn.* **1986**, *55*, 3553–3573.

(125) Takei, W. J.; Cox, D. E.; Shirane, G. Magnetic structures in the MnSb-CrSb system. *Phys. Rev.* **1963**, *129*, 2008–2018.

(126) Velge, W. A. J. J. Magnetic and crystallographic properties of some rare earth cobalt compounds with $CaZn_5$ Structure. *J. Appl. Phys.* **1968**, *39*, 1717.

(127) Fruchart, R.; Roger, A.; Senateur, R. A. Crystallographic and magnetic properties of solid solutions of the phosphides M_2P, M = Cr, Mn, Fe, Co, and Ni. *J. Appl. Phys.* **1969**, *40*, 1250.

(128) Tishin, A. M. Magnetocaloric effect in lanthanide materials. *J. Alloys Compd.* **1997**, *250*, 635–641.

(129) Mandal, K.; Yan, A.; Kerschl, P.; Handstein, A.; Gutfleisch, O.; Müller, K. H. The study of magnetocaloric effect in R_2Fe_{17} (R = Y, Pr) alloys. *J. Phys. D-Applied Phys.* **2004**, *37*, 2628–2631.

(130) Singh, S.; Caron, L.; D'Souza, S. W.; Fichtner, T.; Porcari, G.; Fabbrici, S.; Shekhar, C.; Chadov, S.; Solzi, M.; Felser, C. Large magnetization and reversible magnetocaloric effect at the second-order magnetic transition in Heusler materials. *Adv. Mater.* **2016**, *28*, 3321–3325.

(131) Arrott, A.; Noakes, J. E. Approximate equation of state for nickel near its critical temperature. *Phys. Rev. Lett.* **1967**, *19*, 786–789.

(132) Hill, J.; Mulholland, G.; Persson, K.; Seshadri, R.; Wolverton, C.; Meredig, B. Materials science with large-scale data and informatics: Unlocking new opportunities. *MRS Bull.* **2016**, *41*, 399–409.

(133) Gutfleisch, O.; Gottschall, T.; Fries, M.; Benke, D.; Radulov, I.; Skokov, K. P.; Wende, H.; Gruner, M.; Acet, M.; Entel, P.; Farle, M. Mastering hysteresis in magnetocaloric materials. *Philos. Trans. R. Soc. A Math. Phys. Eng. Sci.* **2016**, *374*, 20150308.

(134) Ward, L.; Wolverton, C. Atomistic calculations and materials informatics: A review. *Curr. Opin. Solid State Mater. Sci.* **2016**, In press.

(135) Jain, A.; Hautier, G.; Ong, S. P.; Persson, K. New opportunities for materials informatics: Resources and data mining techniques for uncovering hidden relationships. *J. Mater. Res.* **2016**, *31*, 977–994.

(136) Kalidindi, S. R.; De Graef, M. Materials data science: Current status and future Outlook. *Annu. Rev. Mater. Res.* **2015**, *45*, 171–193.

(137) Kalidindi, S. R.; Brough, D. B.; Li, S.; Cecen, A.; Blekh, A. L.; Congo, F. Y. P.; Campbell, C. Role of materials data science and informatics in accelerated materials innovation. *MRS Bull.* **2016**, *41*, 596–602.

(138) Gaultois, M. W.; Sparks, T. D.; Borg, C. K. H.; Seshadri, R.; Bonificio, W. D.; Clarke, D. R. Data-driven review of thermoelectric materials: performance and resource considerations. *Chem. Mater.* **2013**, *25*, 2911–2920.

(139) Xu, Y.; Yamazaki, M.; Villars, P. Inorganic materials database for exploring the nature of material. *Jpn. J. Appl. Phys.* **2011**, *50*, 11RH02.

Graphical TOC Entry

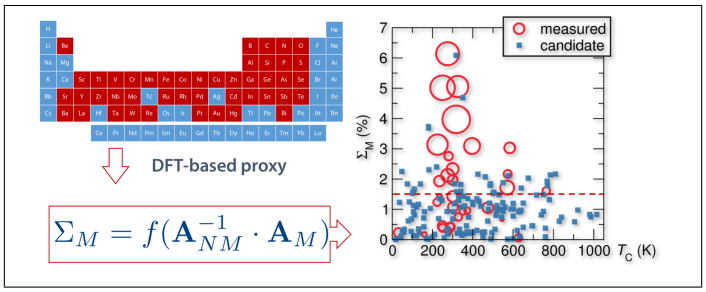

Supporting information:

A Simple Computational Proxy for Screening Magnetocaloric Compounds

Joshua D. Bocarsly,[†,‡] Emily E. Levin,[†,‡] Christina A. C. Garcia,[¶] Kai Schwennicke,[§] Stephen D. Wilson,[‡,†] and Ram Seshadri[*,‡,†,‖]

†*Materials Department, University of California, Santa Barbara, California 93106, United States*

‡*Materials Research Laboratory, University of California, Santa Barbara, California 93106, United States*

¶*Physics Program, College of Creative Studies, University of California, Santa Barbara, California 93106, United States*

§*Chemistry Program, College of Creative Studies, University of California, Santa Barbara, California 93106, United States*

‖*Department of Chemistry and Biochemistry, Santa Barbara, California 93106, United States*

E-mail: seshadri@mrl.ucsb.edu

Sample synthesis and $\Delta S_M(\Delta H, T)$ measurements

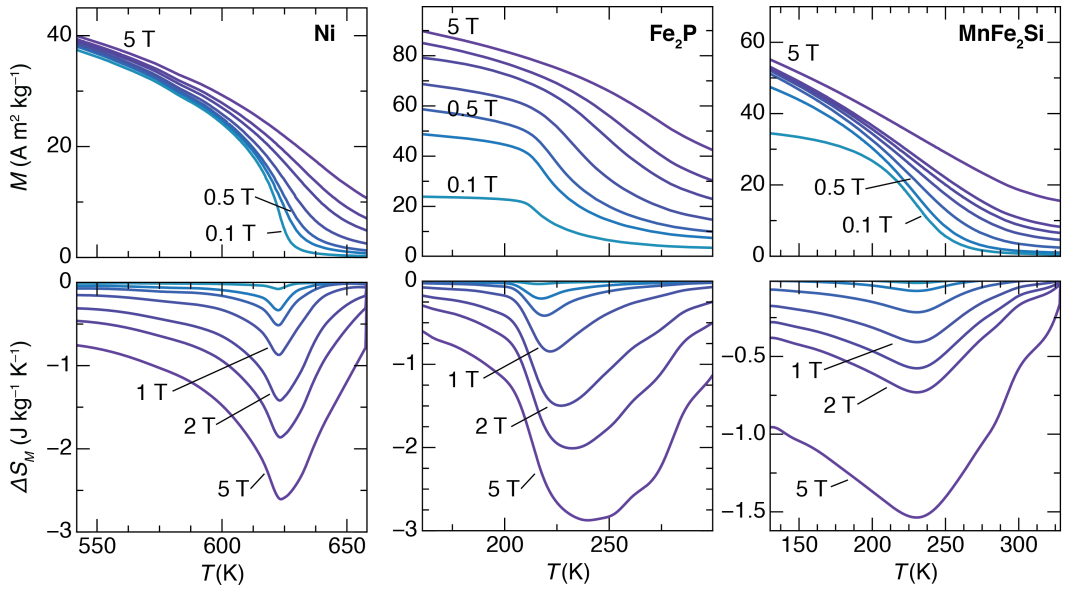

Figure S1: Magnetocaloric characterization of Ni foil, Fe_2P and Heusler $MnFe_2Si$ *via* magnetic measurements. For Ni and Fe_2P, the $M(T)$s were taken at fields of 0.1 T, 0.3 T, 0.5 T, 1 T, 2 T, 3 T, and 5 T. For $MnFe_2Si$, the $M(T)$s were taken at fields of 0.1 T, 0.2 T, 0.5 T, 1 T, 1.5 T, 2 T, and 5 T.

Ni foil (0.125 mm thickness, $\geq$99.9 % purity) and **Fe_2P** powder (99.5% purity) were obtained from Aldrich.

The Heusler **$MnFe_2Si$** was prepared by a rapid assisted microwave synthesis method, which has been shown to be an effective way to synthesize intermetallics.[1] Stoichiometric amounts of Mn, Fe, and Si powders, totaling about 1 g in mass, were weighted and ground together with a mortar and pestle. The powder was pressed into a pellet 6 mm in diameter and sealed in an evacuated silica ampoule which was then placed in an alumina crucible filled with 7 g activated charcoal. The charcoal acts as a microwave susceptor. This crucible was placed in an alumina foam housing, loaded into a 1200 W domestic Panasonic microwave (model NN-SN651B) and heated at 70% power (840 W) for 2.5 minutes and then 90% power (1080 W) for 3 minutes. The resulting compound was annealed in the evacuated ampoule for 5 days at 650°C to promote homogenization of the final product. The sample was confirmed to be the correct phase by laboratory powder X-ray diffraction.

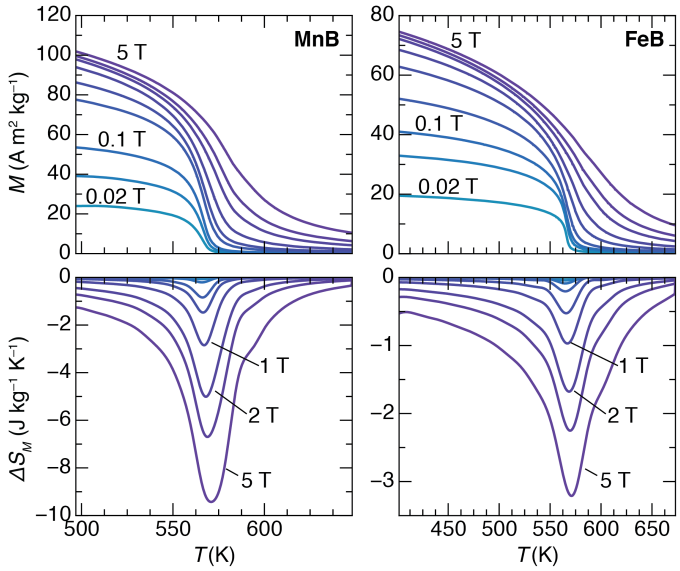

Figure S2: Magnetocaloric characterization of TiNiSi-type MnB and FeB *via* magnetic measurements. For MnB, the $M(T)$s were taken at fields of 0.02 T, 0.05 T, 0.1 T, 0.3 T, 0.5 T, 1 T, 2 T, 3 T, and 5 T. For FeB, the $M(T)$s were taken at fields of 0.02 T, 0.06 T, 0.1 T, 0.2 T, 0.5 T, 1 T, 2 T, 3 T, and 5 T.

The compounds **MnB** and **FeB** were prepared by assisted microwave synthesis, using a procedure similar to $MnFe_2Si$. Stoichiometric amounts of elemental Mn or Fe and B powders were weighed out, including an extra 2 wt.% B to account for losses during heating. The powders were ground and pressed into 300 mg pellets 6 mm in diameter. Each pellets was sealed in an evacuated fused silica ampoule. The ampoule was placed in a crucible with 6.5 g activated charcoal which had been preheated in the microwave to about 150°C, and this was placed in an alumina foam housing. The samples were microwaved at 70% power (840W) for 3 minutes and allowed to cool in the microwave. Melting of the pellet was not observed. Pellets were annealed in evacuated ampoules at 1100°C for 2 days, followed by air quenching. Weight loss of 1.9% was observed in the FeB sample, which we attribute to loss of boron during the microwave step. Formation of FeB and MnB were confirmed by laboratory powder X-ray diffraction.

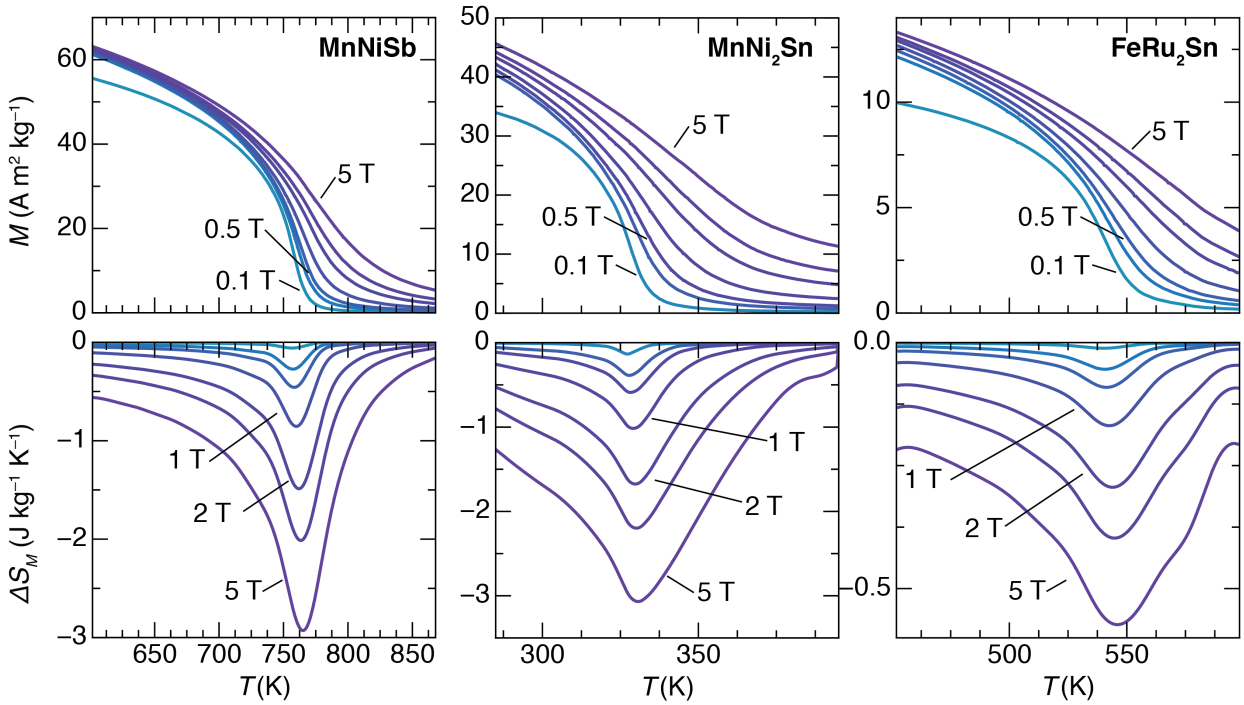

Figure S3: Magnetocaloric characterization of half-Heusler MnNiSb and full-Heuslers $MnNi_2Sn$ and $FeRu_2Sn$ *via* magnetic measurements. The $M(T)$s were taken at fields of 0.1 T, 0.3 T, 0.5 T, 1 T, 2 T, 3 T, and 5 T.

Half-Heusler **MnNiSb** and Heusler **$MnNi_2Sn$** were similarly prepared using assisted microwave synthesis. The pure elements were ground together and pressed into 1 g pellets and then sealed in evacuated silica ampoules and loaded into the microwaves as described for MnB and FeB. MnNiSb was microwaved at 70% power (840 W) for 2.5 minutes and then annealed in the evacuated ampoule at 650°C for 7 days before air quenching. $MnNi_2Sn$ was microwaved for 100% power (1200 W) for 3 minutes and then annealed in the evacuated ampoule at 850°C for 4 days before air quenching. The phases were verified by laboratory X-ray diffraction.

$FeRu_2Sn$ was synthesized as described previously.[2]

Sample synthesis and structural characterization of MnCoP

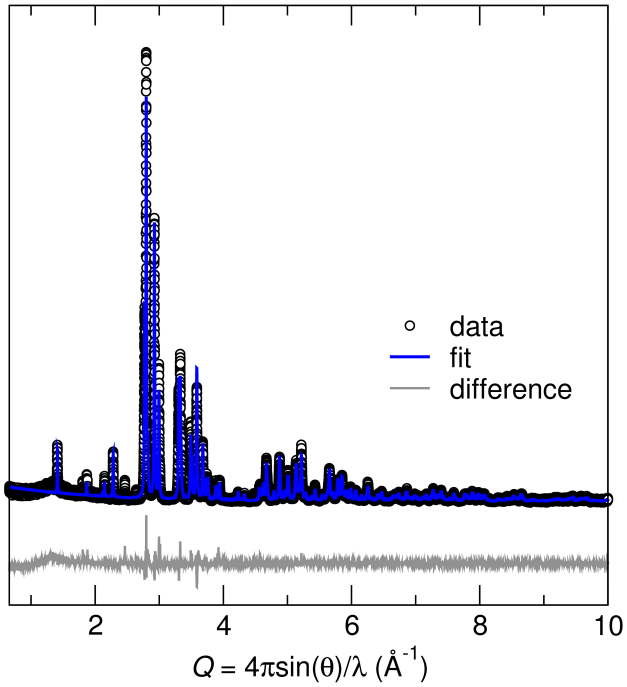

Figure S4: Rietveld refinement of the synchrotron XRD pattern of the MnCoP sample. The pattern shows good agreement with the structural model previously reported (TiNiSi-type, $Pnma$).[3]

MnCoP was made by assisted microwave reaction. Stoichiometric amounts of Mn_3P_2, Co, and red P powders were ground in a mortar and pestle and pressed into a pellet 6 mm in diameter, which was then sealed in an evacuated silica ampoule. The ampoule was placed in an alumina crucible surrounded by 7 g of activated charcoal that had been preheated to 100°C, which acts as a susceptor material in the microwave. This crucible was then placed in a thermally insulating housing made from alumina foam and microwaved at 70% power (840 W) for 2.5 minutes. The silica ampoule was then transferred to a conventional furnace and the sample was annealed at 950°C for 17 hours before quenching in water. The sample was verified to show the $Pnma$ TiNiSi-type structure *via* Rietveld refinement of the synchrotron X-ray diffraction pattern (Figure S4).

Calculation of the magnetic deformation Σ_M

The following Python functions can be used to calculate the degree of lattice deformation between two unit cells. Tested on Python 2.7.10 with NumPy 1.10.1 and Pymatgen 3.2.10. Information on the `pymatgen` package can be found at: `http://pymatgen.org/` .[4]

```
__copyright__ = "Copyright 2017, Joshua D. Bocarsly"
__license__   = "MIT"

from os.path import join as j
import numpy as np
from numpy import linalg as LA
import pymatgen as mg

def magnetic_deformation(nm_struct, m_struct):
    '''
    Calculates the magnetic deformation, which is the degree of lattice
    deformation between an optimized nonmagnetic structure (non spin-polarized)
    and an optimized magnetic structure (spin-polarized).

    nm_struct and m_struct are pymatgen.core.structure.Structure objects
    containing the nonmagnetic optimized cell and the magnetic optimized cell.

    Returns the magnetic deformation expressed as a percentage (float)
    '''
    lmn = nm_struct.lattice_vectors().T
    lm  = m_struct.lattice_vectors().T
    return degree_of_lattice_deformation(lmn, lm)

def degree_of_lattice_deformation(L1, L2):
    '''
    Calculates the degree of lattice deformation between two
    unit cells.

    The unit cells are provided as a 3x3 matrix, with each column containing
    the cartesian representation of one of the lattice vector.

    Returns the degree of lattice deformation as a percentage (float)
    '''
    #calculate the transformation matrix from 1 to 2
    L1_i = LA.inv(L1)
    P = np.dot(L1_i, L2)
    #calculate the lagrangian finite strain tensor, eta
    I = np.identity(3)
    eta = 0.5*(np.dot(P.T,P)-I)
    #calculate the 3 eigenvalues of eta and return the root mean square
    w, v = LA.eig(eta)
    dold = 100*(1./3.)*np.sqrt(w[0]**2 + w[1]**2 + w[2]**2)
    return dold
```

Full datasets

Table S1: Aggregated and computed data for magnetocaloric materials investigated in this study. The Curie temperature (T_C) and peak isothermal entropy change (ΔS_M) columns represent experimental results, either aggregated from literature (top section) or from our own new magnetic measurements (bottom section). The magnetic deformation (Σ_M), saturation magnetization (M_S), percentage volume difference between the magnetic and nonmagnetic cells (ΔV_M), density (ρ), energy of spin polarization (E_{NM-M}), and maximum ionic moment ($\mu_{\max}$), are from DFT calculations performed in the present study. In each case, the ΔS_M is for the ferromagnetic to paramagnetic transition.

	T_C	ΔS_M (J kg^{-1} K^{-1})		ref.	Σ_M	M_s	ΔV_M	ρ	E_{NM-M}	$\mu_{\max}$
	(K)	$H = 2$ T	$H = 5$ T		(%)	(emu/g)	(%)	(g/cm^3)	(eV/atom)	(μ_B)
MnAs	318	−20	−30	5	3.97	121.5	13.2	6.78	0.21	2.9
$MnFeP_{2/3}Si_{1/3}$	250	−16		6	5.02	171.1	7.10	6.67	0.10	2.9
$MnFeGe_{1/3}P_{1/3}Si_{1/3}$	275	−14	−35	7	6.14	154.7	5.80	7.13	0.22	2.9
$MnFeP_{1/3}As_{2/3}$	325	−12	−33	8	5.06	141.7	6.63	7.65	0.20	3.0
$MnFeP_{2/3}As_{1/3}$	225	−11	−16	8	3.14	146.0	7.10	7.22	0.11	3.0
CrO_2	396	−6.8		9	3.09	133.0	3.90	4.83	0.14	2.1
$AlFe_2B_2$	275	−4.5	−7.5	10	2.12	92.3	1.77	5.85	0.03	1.4
Mn_5Ge_3	300	−3.8	−9.4	11	2.33	152.5	11.3	7.49	0.19	3.1
Fe_3C	475	−3.1		12	1.05	170.2	5.53	7.94	0.08	1.9
$LaMnO_3$	300	−3	−7	13	1.43	71.2	7.42	6.55	0.18	2.9
MnCoGe	235	−3	−6	14	1.93	90.7	4.67	8.44	0.17	2.7
Mn_5PB_2	302	−2.6	−5	15	1.08	138.0	4.03	7.01	0.07	1.7
Y_2Fe_{17}	300	−2.5	−4.8	16	1.98	187.3	10.4	7.43	0.15	2.6
Mn_3GaC	250	−2.5	−4.5	17	0.44	95.0	2.31	7.40	0.10	1.8
MnSi	31	−2.2	−3.55	18	0.23	66.9	1.20	5.99	0.03	1.1
Mn_3Sn_2	280	−1.9	−3.5	19	2.76	107.3	8.15	7.91	0.13	2.8
MnP	290	−1.8	−3.8	20	0.41	46.9	1.22	6.17	0.01	0.8
Mn_3AlC	288	−1.6	−3.5	21	0.43	107.0	2.26	6.17	0.09	1.6
$MnNi_2Ga$	329	−1.5		22	0.75	93.7	3.93	8.26	0.31	3.4
Fe_5Si_3	373	−1	−2.8	11	0.96	111.7	3.13	6.70	0.08	1.8
La_2MnNiO_6	280	−1	−2.1	23	0.27	57.2	1.40	7.00	0.19	3.0
MnFeGe	235	−0.75	−1.6	14	1.42	83.8	3.68	8.36	0.20	2.4
$SrRuO_3$	160	−0.6	−2	24	0.17	47.3	0.84	6.31	0.02	1.4
Fe_3GeTe_2	225		−1.1	25	1.24	70.8	6.12	7.00	0.13	2.4
Ni	627	−1.4	−2.5	this work	0.07	55.6	0.34	9.03	0.06	0.6
Fe_2P	223	−1.5	−2.9	—*do.*—	1.23	116.7	3.64	7.15	0.07	2.3
MnB	571	−5.1	−9.4	—*do.*—	1.72	155.1	3.64	6.58	0.09	1.9
FeB	573	−1.7	−3.2	—*do.*—	2.17	96.6	1.52	7.00	0.06	1.3
MnNiSb	765	−1.5	−3	—*do.*—	1.61	94.9	8.50	7.60	0.53	3.7
$MnNi_2Sn$	350	−1.15	−2.1	—*do.*—	0.93	80.0	4.85	8.74	0.36	3.6
$FeRu_2Sn$	545	−0.29	−0.57	—*do.*—	0.67	61.7	3.49	10.4	0.27	3.1
$MnFe_2Si$	250	−1.7	−0.7	—*do.*—	0.39	86.1	2.03	7.46	0.22	2.5
MnCoP	583	−3.1	−6	—*do.*—	3.03	114.9	5.53	7.13	0.13	2.7

Table S2: Experimental Curie temperature T_C and calculated properties for the ferromagnetic candidate materials investigated in this study.

formula	T_C (K)	ref.	Σ_M (%)	M_s (emu/g)	ΔV_M (%)	ρ (g/cm^3)	E_{NM-M} (eV/atom)	$\mu_{\max}$ (μ_B)
Cr_3Te_4	317	26	6.09	83.7	22.67	6.40	0.27	3.4
MnCoAs	350	27	4.69	91.7	7.97	8.15	0.20	3.0
Cr_2Te_3	180	28	3.73	69.3	16.39	6.41	0.32	3.2
MnPtGa	220	29	2.40	65.5	8.22	11.74	0.37	3.7
CrNiAs	182	30	2.31	90.0	7.35	7.64	0.12	3.0
$MnNb_3S_6$	48	31	2.25	45.0	8.42	4.78	0.05	3.9
$Fe_{16}N_2$	810	32	2.17	213.4	11.47	7.73	0.04	2.8
FeCoP	425	27	2.16	78.0	3.28	7.45	0.09	1.8
Fe_5SiB_2	784	33	2.14	147.2	5.00	7.05	0.07	2.1
Fe_3Pd	575	34	2.11	168.8	11.16	8.86	0.27	2.8
Fe_3Pt	462	35	2.07	127.8	10.96	11.65	0.19	2.8
Fe_4CoSiB_2	675	36	2.03	117.9	3.76	7.23	0.05	1.6
Fe_4N	769	32	1.93	232.0	10.20	7.27	0.26	3.0
Fe_3N	550	37	1.88	187.8	6.89	7.48	0.16	2.1
$MnGa_2Sb_2$	310	38	1.85	34.7	4.85	6.85	0.06	2.9
Fe_2CoN	488	39	1.84	155.4	5.90	7.68	0.12	2.2
$MnTa_4S_8$	75	40	1.84	21.7	7.57	7.13	0.05	3.9
CrNiP	140	27	1.84	104.3	5.32	6.70	0.05	2.5
$MnGeAs_2$	340	41	1.82	83.6	9.62	4.84	0.18	3.8
$Fe_{23}Y_6$	485	42	1.79	152.8	9.45	6.98	0.15	2.5
Fe_4MnSiB_2	770	36	1.79	141.5	4.43	7.00	0.08	2.1
Fe_3Ge	640	43	1.70	147.8	7.18	8.37	0.22	2.2
Ba_2MnReO_6	110	44	1.67	35.8	8.81	7.27	0.12	4.3
$MnGe_4$	340	45	1.60	25.2	1.10	6.68	0.02	1.8
$Sr_3Ru_2O_7$	104	46	1.59	39.7	1.89	5.90	0.01	1.4
$MnGeP_2$	320	41	1.58	98.9	8.14	3.93	0.05	3.1
Fe_3RhN	505	47	1.56	168.9	8.24	8.39	0.17	2.6
$MnNb_4S_8$	100	40	1.53	29.7	6.32	4.72	0.04	3.7
MnPdSb	500	48	1.52	66.3	8.01	8.15	0.23	3.2
FePt	750	49	1.49	72.1	7.84	14.91	0.34	2.9
$MnCu_2Sn$	530	50	1.49	72.9	7.83	8.28	0.35	3.7
Fe_3P	716	37	1.47	157.3	5.76	7.44	0.13	2.2
Mn_3ZnC	353	51	1.44	161.7	7.56	6.94	0.14	2.7
$CuCr_2Te_4$	329	52	1.38	44.3	7.27	6.40	0.33	3.0
Fe_2NiN	234	39	1.37	126.3	4.73	7.64	0.13	2.1
$CuCr_2S_4$	375	52	1.36	94.9	7.15	4.13	0.24	2.7
Sr_2FeMoO_6	420	44	1.35	7.3	7.11	5.56	-0.04	0.7
$TaMn_2B_4$	780	53	1.32	66.7	2.34	8.99	0.08	2.1
MnPtSn	330	54	1.30	55.5	6.82	10.25	0.56	3.8

Table S2: Experimental Curie temperature T_C and calculated properties for the ferromagnetic candidate materials investigated in this study.

formula	T_C (K)	ref.	Σ_M (%)	M_s (emu/g)	ΔV_M (%)	ρ (g/cm^3)	E_{NM-M} (eV/atom)	$\mu_{\max}$ (μ_B)
$MnPd_2Sb$	247	50	1.29	62.0	6.79	9.60	0.51	4.0
$CuCr_2Se_4$	430	55	1.27	59.3	6.69	5.71	0.30	2.9
$CdCr_2S_4$	86	56	1.25	97.2	6.55	4.19	0.38	2.9
Fe_3Al	400	57	1.23	169.9	6.48	6.88	0.24	2.4
$HgCr_2S_4$	36	58	1.23	77.3	6.47	5.22	0.36	2.9
Fe_3Y	549	42	1.22	82.4	5.51	7.18	0.10	2.1
Fe_4MnPB_2	650	36	1.21	140.7	4.23	7.19	0.08	2.2
$MnCu_2Al$	600	50	1.20	94.9	6.29	6.68	0.27	3.4
Ba_2FeMoO_6	308	44	1.19	42.8	6.26	6.41	0.10	3.7
$CdCr_2Se_4$	130	56	1.17	63.0	6.14	5.53	0.41	3.0
Sr_2FeReO_6	400	44	1.16	32.7	6.07	6.73	0.10	3.7
$HgCr_2Se_4$	106	58	1.13	53.9	5.93	6.39	0.39	3.0
$MnCu_2In$	520	50	1.13	69.9	5.91	8.33	0.36	3.6
$MnNi_2Sb$	360	50	1.12	75.6	5.86	8.80	0.35	3.6
$CrMn_2B_4$	440	53	1.11	90.9	1.92	6.15	0.04	1.8
$CrTa_3Se_6$	120	31	1.08	16.0	4.08	8.78	0.07	3.1
WMn_2B_4	560	53	1.07	58.4	1.26	9.37	0.06	1.8
$MnNi_2Sn$	344	50	1.07	78.7	5.61	8.71	0.35	3.6
$MnPd_2Sn$	189	50	1.03	60.1	5.41	9.73	0.49	3.9
Fe_7C_3	523	59	1.02	151.3	3.71	7.86	0.07	2.0
$MoMn_2B_4$	590	53	1.01	78.7	1.54	6.96	0.06	1.8
Fe_2Zr	600	60	1.01	84.3	5.30	7.80	0.11	2.0
$ScFe_2$	545	61	1.00	94.2	3.80	6.23	0.09	1.8
MnCoSb	478	54	1.00	70.9	5.24	7.98	0.38	3.2
Co_5Y	921	62	0.98	105.2	4.82	7.72	0.11	1.6
Fe_5PB_2	640	36	0.97	143.1	4.94	7.26	0.07	2.0
Mn_5SiB_2	628	33	0.94	131.5	3.64	6.83	0.07	1.7
Fe_5C_2	519	63	0.93	153.2	4.81	7.83	0.09	2.1
Fe_2Y	550	64	0.93	86.0	4.89	7.04	0.17	2.0
Ni_3Mn	750	32	0.93	119.4	4.88	8.52	0.26	3.2
Mn_3InC	272	65	0.93	116.0	4.88	7.89	0.13	2.5
$CrNb_3S_6$	160	31	0.92	32.1	3.73	4.90	0.06	2.8
Ba_2FeReO_6	303	44	0.92	27.3	4.82	7.50	0.14	3.7
$CrNb_3Se_6$	105	31	0.92	21.1	3.43	6.57	0.08	3.0
$ZrFe_2$	633	66	0.91	83.7	4.79	7.85	0.11	2.0
$FeCo_2Ge$	980	67	0.83	126.1	4.35	8.74	0.32	2.9
$FeCo_2Si$	1015	67	0.83	148.9	4.34	7.58	0.30	2.8
Fe_3Ge	740	43	0.82	125.2	4.27	8.60	0.28	2.6
$BaFeO_3$	110	68	0.81	83.8	4.25	6.42	0.22	3.0

Table S2: Experimental Curie temperature T_C and calculated properties for the ferromagnetic candidate materials investigated in this study.

formula	T_C (K)	ref.	Σ_M (%)	M_s (emu/g)	ΔV_M (%)	ρ (g/cm^3)	E_{NM-M} (eV/atom)	$\mu_{\max}$ (μ_B)
Fe_4CoPB_2	515	36	0.80	108.6	3.51	7.46	0.05	1.6
Fe_3Si	600	69	0.78	146.0	4.07	7.42	0.25	2.6
$MnCo_2Si$	985	50	0.75	138.9	3.94	7.51	0.36	3.0
$MnNi_2Ga$	379	50	0.74	93.7	3.89	8.26	0.31	3.4
$FePd_3$	543	35	0.74	63.5	3.88	10.65	0.35	3.3
CoPt	840	70	0.74	49.0	3.12	15.73	0.16	1.9
Co_2B	156	71	0.72	83.1	1.02	8.23	0.05	1.0
La_2MnCoO_6	230	72	0.69	68.7	3.58	6.82	0.15	2.9
FeNiP	95	27	0.68	45.6	1.46	7.37	0.05	1.4
FeCoAs	300	27	0.68	64.5	2.95	8.51	0.14	2.1
$MnTa_3S_6$	80	31	0.62	12.6	1.27	7.78	0.01	1.8
Co_3B	474	71	0.61	105.6	2.09	8.35	0.08	1.3
$MnCo_2Sn$	829	50	0.61	96.5	3.17	9.07	0.43	3.2
$MnCo_2Ge$	905	50	0.59	113.7	3.07	8.69	0.39	3.1
$MnCo_2Al$	697	73	0.46	112.6	2.39	7.21	0.31	2.7
Fe_3ZnC	368	51	0.46	93.8	2.38	7.60	0.11	1.7
$MnCo_2Ga$	694	50	0.45	94.3	2.37	8.67	0.32	2.8
MnB_2	157	74	0.42	133.3	1.71	5.63	0.14	1.8
MnAl	650	32	0.41	129.8	1.99	5.35	0.17	1.9
VMn_2Al	760	73	0.38	59.5	1.97	6.38	0.06	1.4
CoS_2	130	75	0.36	45.2	1.86	4.92	0.01	0.9
$BaRuO_3$	60	76	0.34	43.3	1.80	7.11	0.02	1.5
$CrCo_2Al$	334	73	0.34	85.2	1.79	7.06	0.12	1.6
Fe_3GaC	510	51	0.34	70.1	1.78	7.80	0.04	1.2
Sr_2CrMoO_6	420	44	0.31	26.7	1.60	5.73	0.07	0.5
Sr_2CrReO_6	620	44	0.31	10.8	1.59	6.96	0.07	1.1
$CrBe_{12}$	50	77	0.29	47.4	1.06	2.49	0.01	1.7
VCo_2Sn	95	73	0.27	57.3	1.42	8.80	0.06	1.1
Sr_2CrWO_6	458	44	0.25	22.0	1.31	6.86	0.07	2.3
$TiCo_2Sn$	371	78	0.25	39.4	1.30	8.40	0.04	1.1
$HfCo_2Sn$	394	79	0.25	26.9	1.28	11.31	0.04	1.1
VCoSb	58	80	0.24	24.1	1.27	7.80	0.04	1.2
$ZrCo_2Sn$	448	79	0.24	34.1	1.26	8.80	0.05	1.1
$CrCo_2Ga$	495	73	0.23	70.5	1.22	8.54	0.13	1.6
$CoPt_3$	400	70	0.23	25.2	1.19	18.36	0.11	2.0
Mn_3GeC	330	51	0.22	65.1	1.14	7.61	0.08	1.2
TiCoSn	134	81	0.21	9.2	1.10	6.50	0.00	0.6
$MnNi_2In$	323	50	0.21	81.3	1.08	8.95	0.36	3.5
$TiCo_2Ge$	384	78	0.20	47.2	1.07	7.96	0.04	1.0

Table S2: Experimental Curie temperature T_C and calculated properties for the ferromagnetic candidate materials investigated in this study.

formula	T_C (K)	ref.	Σ_M (%)	M_s (emu/g)	ΔV_M (%)	ρ (g/cm^3)	E_{NM-M} (eV/atom)	$\mu_{\max}$ (μ_B)
VCo_2Ga	358	82	0.19	46.8	0.99	8.32	0.05	0.9
$CrFe_2Al$	210	57	0.18	5.0	0.93	7.00	0.00	0.2
$NbCo_2Sn$	105	79	0.13	29.0	0.68	9.32	0.02	0.9
$TiCo_2Al$	120	83	0.13	28.8	0.65	6.47	0.01	0.6
Au_4V	44	84	0.12	12.7	0.56	16.36	0.06	1.8
MnBi	633	32	0.10	60.4	0.44	11.15	0.08	2.9
Ni_3Pt	450	70	0.10	34.8	0.51	12.70	0.04	0.8
FePd	760	49	0.09	110.2	0.46	10.48	0.39	2.9
NiPt	200	70	0.09	23.4	-0.46	15.85	0.01	0.7
Ni_3Al	41.5	84	0.08	22.2	0.40	7.47	0.00	0.3
WMn_2Sn	258	73	0.06	0.0	0.33	12.07	0.00	0.0
$CrTa_3S_6$	170	31	0.03	21.7	0.15	7.70	0.04	2.7
MnSb	600	85	0.03	73.0	0.12	8.35	0.00	2.4
Co_7La_2	490	86	0.02	2.2	0.03	7.86	0.00	0.4
$Co_3Sn_2S_2$	177	59	0.02	11.6	-0.08	7.23	0.01	0.4
MnPtSb	572	54	0.01	58.2	-0.07	11.20	0.20	3.6
$ZrZn_2$	17	84	0.01	22.1	0.05	7.31	0.02	0.5

References

(1) Birkel, C. S.; Zeier, W. G.; Douglas, J. E.; Lettiere, B. R.; Mills, C. E.; Seward, G.; Birkel, A.; Snedaker, M. L.; Zhang, Y.; Snyder, G. J.; Pollock, T. M.; Seshadri, R.; Stucky, G. D. Rapid microwave preparation of thermoelectric TiNiSn and TiCoSb half-Heusler compounds. *Chem. Mater.* **2012**, *24*, 2558–2565.

(2) Douglas, J. E.; Levin, E. E.; Pollock, T. M.; Castillo, J. C.; Adler, P.; Felser, C.; Krämer, S.; Page, K. L.; Seshadri, R. Magnetic hardening and antiferromagnetic/ferromagnetic phase coexistence in $Mn_{1-x}Fe_xRu_2Sn$ Heusler solid solutions. *Phys. Rev. B* **2016**, *94*, 094412.

(3) Fruchart, R.; Roger, A.; Senateur, R. A. Crystallographic and magnetic properties of solid solutions of the phosphides M_2P, M = Cr, Mn, Fe, Co, and Ni. *J. Appl. Phys.* **1969**, *40*, 1250.

(4) Ong, S. P.; Richards, W. D.; Jain, A.; Hautier, G.; Kocher, M.; Cholia, S.; Gunter, D.; Chevrier, V. L.; Persson, K. A.; Ceder, G. Python Materials Genomics (pymatgen): A robust, open-source python library for materials analysis. *Comput. Mater. Sci.* **2013**, *68*, 314–319.

(5) Wada, H.; Tanabe, Y. Giant magnetocaloric effect of $MnAs_{1-x}Sb_x$. *Appl. Phys. Lett.* **2001**, *79*, 3302.

(6) Katagiri, K.; Nakamura, K.; Wada, H. Magnetocaloric properties and magnetic refrigerant capacity of $MnFeP_{1-x}Si_x$. *J. Alloys Compd.* 286–290.

(7) Thanh, D. T. C.; BrüÂĹck, E.; Tegus, O.; J. C. P., K.; Gortenmulder, T. J.; Buschow, K. H. J. Magnetocaloric effect in MnFe(P,Si,Ge) compounds. *J. Appl. Phys.* **2006**, *99*, 08Q107.

(8) Tegus, O.; Brück, E.; Zhang, L.; Dagula,; Buschow, K. H. J.; de Boer, F. R. Magnetic-phase transitions and magnetocaloric effects. *Physica B: Condensed Matter* **2002**, *319*, 174–192.

(9) Zhang, X.; Chen, Y.; Lü, L.; Li, Z. A potential oxide for magnetic refrigeration application: CrO_2 particles. *J. Phys.: Condensed Matter* **2006**, *18*, L559–L566.

(10) Tan, X.; Chai, P.; Thompson, C. M.; Shatruk, M. Magnetocaloric effect in $AlFe_2B_2$: toward Magnetic refrigerants from earth-abundant elements. *J. Am. Chem. Soc.* **2013**, *135*, 9553–9557.

(11) Songlin,; Dagula,; Tegus, O.; Brück, E.; Klaasse, J. C. P.; de Boer, F.; Buschow, K. Magnetic phase transition and magnetocaloric effect in $Mn_{5-x}Fe_xSi_3$. *J. Alloys Compd.* **2002**, *334*, 249–252.

(12) Kaeswurm, B.; Friemert, K.; Gürsoy, M.; Skokov, K. P.; Gutfleisch, O. Direct measurement of the magnetocaloric effect in cementite. *J. Magn. Magn. Mater.* **2016**, *410*, 105–108.

(13) Phan, M.-H.; Yu, S.-C. Review of the magnetocaloric effect in manganite materials. *J. Magn. Magn. Mater.* **2007**, *308*, 325–340.

(14) Lin, S.; Tegus, O.; Brück, E.; Dagula, W.; Gortenmulder, T.; Buschow, K. Structural and magnetic properties of $MnFe_{1-x}Co_xGe$ Compounds. *IEEE Trans. Magn.* **2006**, *42*, 3776–3778.

(15) Xie, Z. G.; Geng, D. Y.; Zhang, Z. D. Reversible room-temperature magnetocaloric effect in Mn_5PB_2. *Appl. Phys. Lett.* **2010**, *97*, 202504.

(16) Llamazares, J. S.; Álvarez-Alonso, P.; Sánchez-Valdés, C.; Ibarra-Gaytán, P. J.; Blanco, J. A.; Gorria, P. Investigating the magnetic entropy change in single-phase Y_2Fe_{17} melt-spun ribbons. *Curr. Appl. Phys.* **2016**, *16*, 963–968.

(17) Tong, P.; Wang, B.-S.; Sun, Y.-P. Mn-based antiperovskite functional materials: Review of research. *Chin. Phys. B.* **2013**, *22*, 067501.

(18) Arora, P.; Chattopadhyay, M. K.; Roy, S. B. Magnetocaloric effect in MnSi. *Appl. Phys. Lett.* **2007**, *91*, 062508.

(19) Recour, Q.; Mazet, T.; Malaman, B. Magnetocaloric properties of Mn_3Sn_2 from heat capacity measurements. *J. Appl. Phys.* **2009**, *105*, 033905.

(20) Booth, R. A.; Majetich, S. A. Crystallographic orientation and the magnetocaloric effect in MnP. *J. Appl. Phys.* **2009**, *105*, 07A926.

(21) Tong, P.; Wang, B.-S.; Sun, Y.-P. Mn-based antiperovskite functional materials: Review of research. *Chin. Phys. B.* **2013**, *22*, 067501.

(22) Tegus, O.; Brück, E.; Zhang, L.; Dagula,; Buschow, K. H. J.; de Boer, F. R. Magnetic-phase transitions and magnetocaloric effects. *Physica B: Condensed Matter* **2002**, *319*, 174–192.

(23) Balli, M.; Fournier, P.; Jandl, S.; Gospodinov, M. M. A study of the phase transition and magnetocaloric effect in multiferroic La_2MnNiO_6 single crystals. *J. Appl. Phys.* **2014**, *115*, 173904.

(24) Zhang, X.-Y.; Chen, Y.; Li, Z.-Y. Magnetocaloric effect in 4d itinerant ferromagnet $SrRuO_3$. *J. Alloys Compd.* **2008**, *459*, 51–54.

(25) Verchenko, V. Y.; Tsirlin, A. A.; Sobolev, A. V.; Presniakov, I. A.; Shevelkov, A. V. Ferromagnetic order, strong magnetocrystalline anisotropy, and magnetocaloric effect in the layered telluride $Fe_{3-\delta}GeTe_2$. *Inorg. Chem.* **2015**, *54*, 8598–8607.

(26) Akram, M.; Nazar, F. M. Magnetic properties of CrTe, $Cr_{23}Te_{24}$, Cr_7Te_8, Cr_5Te_6, and Cr_3Te_4 compounds. *J. Mater. Sci.* **1983**, *18*, 423–429.

(27) Nylund, M. A.; Roger, M. M. A.; Sénateur, J. P.; Fruchart, R. Evolution structurale des phosphures, arséniures et arséniophosphures M_2P, M_2As et $M_2(P_{1-x}As_x)$. *J. Solid State Chem.* **1972**, *4*, 115–122.

(28) Yuzuri, M.; Kanomata, T.; Kaneko, T. The pressure effect on the Curie temperature and exchange striction of Cr_2S_3 and Cr_2Te_3. *J. Magn. Magn. Mater.* **1987**, *70*, 223–224.

(29) Buschow, K. H. J.; Mooij, D. B. D. Crystal structure and magnetic properties of PtMnGa and PtMnAl. *J. Less Common Met.* **1984**, *99*, 125–130.

(30) Bacmann, M.; Fruchart, D.; Koumina, A.; Wolfers, P. Low temperature magnetic structure of CrNiAs. *Mater. Sci. Forum* **2004**, *443-444*, 379–382.

(31) Hulliger, F.; Pobitschka, E. On the magnetic behavior of new 2H-NbS_2-type derivatives. *J. Solid State Chem.* **1970**, *1*, 117–119.

(32) Coey, J. M. D. *Magnetism and Magnetic Materials*; Magnetism and Magnetic Materials; Cambridge University Press, 2010.

(33) R, W.; Ericsson, T.; Häggström, L.; Andersson, Y. Magnetic properties of Fe_5SiB_2 and related compounds. *J. Phys. Colloq.* **1976**, *37*, C6–591–C6–593.

(34) Cui, J.; James, R. D. Study of Fe_3Pd and related alloys for ferromagnetic shape memory. *IEEE Trans. Magn.* **2001**, *37*, 2675–2677.

(35) Seeger, M.; Kronmüller, H. The magnetic phase transition in ordered and disordered ferromagnets. *J. Magn. Magn. Mater.* **1989**, *78*, 393–402.

(36) McGuire, M. A.; Parker, D. S. Magnetic and structural properties of ferromagnetic Fe_5PB_2 and Fe_5SiB_2 and effects of Co and Mn substitutions. *J. Appl. Phys.* **2015**, *118*, 163903.

(37) Gambino, R. J. Magnetic properties of the iron-group metal phosphides. *J. Appl. Phys.* **1967**, *38*, 1253.

(38) Sakakibara, W.; Hayashi, Y.; Takizawa, H. $MnGa_2Sb_2$, a new ferromagnetic compound synthesized under high pressure. *J. Ceram. Soc. Jpn.* **2009**, *117*, 72–75.

(39) Guo, K.; Rau, D.; Toffoletti, L.; Müller, C.; Burkhardt, U.; Schnelle, W.; Niewa, R.; Schwarz, U. Ternary metastable nitrides ϵ-Fe_2TMN (TM = Co, Ni): High-pressure, high-temperature synthesis, crystal structure, thermal stability, and magnetic properties. *Chem. Mater.* **2012**, *24*, 4600–4606.

(40) Ōnuki, Y.; Ina, K.; Hirai, T.; Komatsubara, T. Magnetic properties of intercalation compound: $Mn_{1/4}MX_2$. *J. Phys. Soc. Jpn.* **1986**, *55*, 347–356.

(41) Cho, S.; Choi, S.; Cha, G.-B.; Hong, S. C.; Kim, Y.; Freeman, A. J.; Ketterson, J. B.; Park, Y.; Park, H.-M. Synthesis of new pure ferromagnetic semiconductors: $MnGeP_2$ and $MnGeAs_2$. *Solid State Commun.* **2004**, *129*, 609–613.

(42) Buschow, K. H. J. Hydrogen absorption and its effect on the magnetic properties of rare-earth iron intermetallics. *Solid State Commun.* **1976**, *19*, 421–423.

(43) Drijver, J. W.; Sinnema, S. G.; van der Woude, F. Magnetic properties of hexagonal and cubic Fe_3Ge. *J. Phys. F.* **1976**, *6*, 2165–2177.

(44) Serrate, D.; Teresa, J. M. D.; Ibarra, M. R. Double perovskites with ferromagnetism above room temperature. *J. Phys.: Condensed Matter* **2006**, *19*, 023201.

(45) Takizawa, H.; Sato, T.; Endo, T.; Shimada, M. High pressure synthesis and electrical and magnetic properties of $MnGe_4$ and $CoGe_4$. *J. Solid State Chem.* **1990**, *88*, 384–390.

(46) Cao, G.; McCall, S.; Crow, J. E. Observation of itinerant ferromagnetism in layered $Sr_3Ru_2O_7$ single crystals. *Phys. Rev. B.* **1997**, *55*, R672–R675.

(47) Houben, A.; Müller, P.; von Appen, J.; Lueken, H.; Niewa, R.; Dronskowski, R. Synthesis, crystal structure, and magnetic properties of the semihard Itinerant Ferromagnet $RhFe_3N$. *Angew. Chem.* **2005**, *44*, 7212–7215.

(48) Endo, K. Magnetic studies of $C1_b$-Compounds CuMnSb, PdMnSb and Cu_{1-x}(Ni or Pd)$_x$MnSb. *J. Phys. Soc. Jpn.* **1970**, *29*, 643–649.

(49) Klemmer, T.; Hoydick, D.; Okumura, H.; Zhang, B.; Soffa, W. A. Magnetic hardening and coercivity mechanisms in $L1_0$ ordered FePd ferromagnets. *Scripta Metal. Mater.* **1995**, *33*, 1793–1805.

(50) Webster, P. J. Heusler alloys. *Contemp. Phys.* **1969**, *10*, 559–577.

(51) Grandjean, F.; Gerard, A. Study by Mossbauer spectroscopy of the series of perovskite carbides M_3M'C with M=Fe or Mn, and M'=Al, Ga, Ge, Zn, Sn. *J. Phys. F.* **1976**, *6*, 451–467.

(52) Miyatani, K.; Wada, Y.; Okamoto, F. Magnetic properties of single crystal chalcogenide spinels; $CuCr_2X_3Y$ (X = S, Se and Te, Y = Cl, Br and I) system. *J. Phys. Soc. Jpn.* **1968**, *25*, 369–372.

(53) Iga, A.; Tawara, Y. Magnetic properties of molybdenum- and wolfram-Modified Mn_3B_4. *J. Phys. Soc. Jpn.* **1968**, *24*, 28–35.

(54) Irkhin, V. Y.; Katsnel'son, M. I. Half-metallic ferromagnets. *Phys. Uspekhi* **1994**, *37*, 659–676.

(55) Nakatani, I.; Nosé, H.; Masumoto, K. Magnetic properties of $CuCr_2Se_4$ single crystals. *J. Phys. Chem. Solids* **1978**, *39*, 743–749.

(56) Menyuk, N. Ferromagnetism in $CdCr_2Se_4$ and $CdCr_2S_4$. *J. Appl. Phys.* **1966**, *37*, 1387.

(57) Shull, R. D.; Okamoto, H.; Beck, P. A. Transition from ferromagnetism to mictomagnetism in Fe-Al alloys. *Solid State Commun.* **1976**, *20*, 863–868.

(58) Wojtowicz, P. Semiconducting ferromagnetic spinels. *IEEE Trans. Magn.* **1969**, *5*, 840–848.

(59) Tsuzuki, A.; Sago, S.; Hirano, S. I.; Naka, S. High temperature and pressure preparation and properties of iron carbides Fe_7C_3 and Fe_3C. *J. Mater. Sci.* **1984**, *19*, 2513–2518.

(60) Mattern, N.; Zhang, W. X.; Roth, S.; Reuther, H.; Baehtz, C.; Richter, M. Structural and magnetic properties of non-stoichiometric Fe_2Zr. *J. Phys.: Condensed Matter* **2007**, *19*, 376202.

(61) Sankar, S. G.; Wallace, W. E. Magnetic properties of $ScFe_2$. AIP Conf. Proc. 1976.

(62) Chikazumi, S. *Physics of Ferromagnetism 2e*; Int. Ser. Monogr. Phys.; OUP Oxford, 2009.

(63) Zhang, Z.-D.; Kershaw, R.; Dwight, K.; Wold, A. Preparation and characterization of nickel substituted Fe_5C_2. *Mater. Res. Bull.* **1986**, *21*, 979–983.

(64) Buschow, K. H. J.; van Diepen, A. M. Effect of hydrogen absorption on the magnetic properties of YFe_2 and $GdFe_2$. *Solid State Commun.* **1976**, *19*, 79–81.

(65) Kanomata, T.; Kaneko, T.; Nakagawa, Y. Magnetic properties of the intermetallic compound Mn_3InC. *J. Solid State Chem.* **1992**, *96*, 451–454.

(66) Marei, S. A.; Craig, R. S.; Wallace, W. E.; Tsuchida, T. Magnetic characteristics of some Laves phase systems containing Fe and Mn. *J. Less Common Met.* **1967**, *13*, 391–398.

(67) Deka, B.; Kundu, A.; Ghosh, S.; Srinivasan, A. Experimental and *ab initio* studies on sub-lattice ordering and magnetism in $Co_2Fe(Ge_{1-x}Si_x)$ alloys. *J. Appl. Phys.* **2015**, *118*, 133906.

(68) Hayashi, N.; Yamamoto, T.; Kageyama, H.; Nishi, M.; Watanabe, Y.; Kawakami, T.; Matsushita, Y.; Fujimori, A.; Takano, M. $BaFeO_3$: A ferromagnetic iron oxide. *Angew. Chem.* **2011**, *50*, 12547–12550.

(69) Shinjo, T.; Nakamura, Y.; Shikazono, N. Magnetic study of Fe_3Si and Fe_5Si_3 by Mössbauer effect. *J. Phys. Soc. Jpn.* **1963**, *18*, 797–801.

(70) Cadeville, M. C.; Dahmani, C. E.; Kern, F. Magnetism and spatial order in Ni-Pt and Co-Pt alloys. *J. Magn. Magn. Mater.* **1986**, *54-57*, 1055–1056.

(71) Zhurakovskii, E. A.; Shashkina, T. B.; Kotlyar, V. I. X-ray absorption spectra of cobalt in ferromagnetic borides. *Soviet Phys. J.* **1970**, *13*, 14–17.

(72) Barón-González, A. J.; Frontera, C.; García-Muñoz, J. L.; Blasco, J.; Ritter, C. Cation order and structural transition in La_2MnCoO_6. *J. Phys.: Conf. Ser.* **2011**, *325*, 012007.

(73) Kübler, J.; Fecher, G. H.; Felser, C. Understanding the trend in the Curie temperatures of Co_2-based Heusler compounds: *Ab initio* calculations. *Phys. Rev. B* **2007**, *76*.

(74) Cadeville, M. C. Proprietes magnetiques des diborures de manganese et de chrome: MnB_2 et CrB_2. *J. Phys. Chem. Solids* **1966**, *27*, 667–670.

(75) Miyahara, S. Magnetic properties of FeS_2 and CoS_2. *J. Appl. Phys.* **1968**, *39*, 896.

(76) Jin, C. Q.; Zhou, J. S.; Goodenough, J. B.; Liu, Q. Q.; Zhao, J. G.; Yang, L. X.; Yu, Y.; Yu, R. C.; Katsura, T.; Shatskiy, A.; Ito, E. High-pressure synthesis of the cubic perovskite $BaRuO_3$ and evolution of ferromagnetism in $A\mathrm{RuO}_3$ (A = Ca, Sr, Ba) ruthenates. *Proc. Natl. Acad. Sci.* **2008**, *105*, 7115–7119.

(77) Wolcott, N. M.; Falge, R. L. Ferromagnetism of $CrBe_{12}$. *Phys. Rev.* **1968**, *171*, 591–595.

(78) Bainsla, L.; Suresh, K. G. Spin polarization studies in half-metallic $Co_2Ti\mathrm{X}$ (X = Ge and Sn) Heusler alloys. *Curr. Appl. Phys.* **2016**, *16*, 68–72.

(79) van Engen, P. G.; Buschow, K. H. J.; Erman, M. Magnetic properties and magneto-optical spectroscopy of Heusler alloys based on transition metals and Sn. *J. Magn. Magn. Mater.* **1983**, *30*, 374–382.

(80) Terada, M.; Endo, K.; Fujita, Y.; Kimura, R. Magnetic Properties of $C1_b$ Compounds; CoVSb, CoTiSb and NiTiSb. *J. Phys. Soc. Jpn.* **1972**, *32*, 91–94.

(81) Kouacou, M. A.; Pierre, J.; Skolozdra, R. V. Semiconductor-metal transition and the onset of itinerant ferromagnetism in the Heusler phases TiCoSn-TiCoSb. *J. Phys.: Condensed Matter* **1995**, *7*, 7373–7385.

(82) Nishihara, H.; Furutani, Y.; Wada, T.; Kanomata, T.; Kobayashi, K.; Kainuma, R.; Ishida, K.; Yamauchi, T. Magnetization process near the Curie temperature of a ferromagnetic Heusler Alloy Co_2VGa. *J. Supercond. Novel Magn.* **2010**, *24*, 679–681.

(83) Pal, L.; Gupta, S.; Suresh, K. Structural and magnetic properties of $Co_2Ti_{1-x}Fe_xAl$ ($0 \leq x \leq 0.5$) Alloys. AIP Conf. Proc. 2014; pp 1526–1528.

(84) Takahashi, Y. On the origin of the Curie-Weiss law of the magnetic susceptibility in itinerant electron ferromagnetism. *J. Phys. Soc. Jpn.* **1986**, *55*, 3553–3573.

(85) Takei, W. J.; Cox, D. E.; Shirane, G. Magnetic structures in the MnSb-CrSb system. *Phys. Rev.* **1963**, *129*, 2008–2018.

(86) Velge, W. A. J. J. Magnetic and crystallographic properties of some rare earth cobalt compounds with $CaZn_5$ Structure. *J. Appl. Phys.* **1968**, *39*, 1717.